Identification of a Novel Endoplasmic Reticulum Export Motif within the Eighth α-Helical Domain (α-H8) of the human Prostacyclin Receptor.

Peter D. Donnellan, Cisca C. Kimbembe, Helen M. Reid and B. Therese Kinsella*

School of Biomolecular and Biomedical Sciences, Conway Institute of Biomolecular Research, University College Dublin, Belfield, Dublin 4, Ireland.
*Corresponding author: Tel: 353-1-7166727; Fax: 353-1-7166454;
Email: Therese.Kinsella@UCD.IE

Running Title: ER Export Motif in α-H8 of the Prostacyclin Receptor

Key Words: GPCR, prostacyclin receptor, alpha helix 8, trafficking, endoplasmic reticulum, export

Abbreviations:

α-H8, α-helix 8; AC, adenylyl cyclase; $[Ca^{2+}]_i$; intracellular calcium; C-tail, carboxyl-terminal tail; COPII vesicles, coat protein-II vesicles; ER, endoplasmic reticulum; ERAD, ER-associated degradation; EC, extracellular; GPCR, G protein-coupled receptor; HA, hemagglutinin; HEK, human embryonic kidney; hIP, human IP; IC, intracellular; IP, PGI_2 receptor; PG, prostaglandin; PM, plasma membrane; RBD, Rab11 binding domain; TM, transmembrane.

Abstract

The human prostacyclin receptor (hIP) undergoes agonist-dependent trafficking involving a direct interaction with Rab11a GTPase. The region of interaction was localised to a 14 residue Rab11a binding domain (RBD) within the proximal carboxyl-terminal (C)-tail domain of the hIP, consisting of Val^{299} – Val^{307} within the eighth helical domain (α-H8) adjacent to the palmitoylated residues at Cys^{308} – Cys^{311}. However, the factors determining the anterograde transport of the newly synthesised hIP from the endoplasmic reticulum (ER) to the plasma membrane (PM) have not been identified. The aim of the current study was to identify the major ER export motif(s) within the hIP initially by investigating the role of Lys residues in its maturation and processing. Through site-directed and *Ala-scanning* mutational studies in combination with analyses of protein expression and maturation, functional analyses of ligand binding, agonist-induced intracellular signalling and confocal image analyses, it was determined that Lys^{297}, Arg^{302} and Lys^{304} located within α-H8 represent the critical determinants of a novel ER export motif of the hIP. Furthermore, while substitution of those critical residues significantly impaired maturation and processing of the hIP, replacement of the positively charged Lys with Arg residues, and *vice versa*, was functionally permissible. Hence, this study has identified a novel 8 residue ER export motif within the functionally important α-H8 of the hIP. This ER export motif, defined by 'K/R$(X)_4$K/R(X)K/R', has a strict requirement for positively charged, basic Lys/Arg residues at the 1^{st}, 6^{th} and 8^{th} positions and appears to be evolutionarily conserved within IP sequences from mouse to man.

1. Introduction

G protein-coupled receptors (GPCRs), the largest superfamily of cell surface receptors, play an integral role in signal transduction [1, 2]. They recognise and bind an array of extracellular stimuli transducing signals to a variety of intracellular effector systems to modulate a host of biological responses [3]. All GPCRs share a common topographical structure characterised by an amino (N)-terminal extracellular domain, seven transmembrane (TM)-spanning α helices linked by three alternating intracellular $(IC)_{1-3}$ and three extracellular $(EC)_{1-3}$ loops and a divergent intracellular carboxyl terminal (C)-tail domain. Additionally, through recent X-ray crystallographic data along with other experimental and computational approaches, the presence of an eighth alpha helical domain (α-H8) within the proximal C-tail domain, adjacent to TM7, has now been recognised as a common structural feature in many GPCRs [4, 5]. Moreover, the α-H8 is both functionally important and diverse, having being implicated in the regulation of receptor -expression and intracellular trafficking, -G-protein coupling and activation, -agonist-induced internalisation and/or -dimerisation [6-10].

The prostanoid prostacyclin, or prostaglandin I_2, mainly produced by the vascular endothelium [11], is a potent proinflammatory mediator [12, 13] and plays a central role in haemostasis, inhibiting platelet aggregation and inducing vasodilation [14, 15]. Prostacyclin exerts an important cytoprotective role within the myocardium [16] and also limits restenosis, promoting vascular repair in response to injury [17]. Stable prostacyclin analogues are used clinically in the treatment of pulmonary arterial hypertension [18]. Prostacyclin mainly signals through interaction with the prostacyclin receptor, or IP, a member of the GPCR superfamily. The IP is abundantly expressed throughout the vasculature, in the heart, kidney, lung, thymus and spleen and in the sensory neurons of the dorsal root ganglion [15, 19]. Alterations in the levels of prostacyclin or of the IP have been implicated in a number of cardiovascular disorders including myocardial infarction, thrombosis, atherosclerosis and restenosis [14, 20, 21]. Additionally, several single nucleotide polymorphisms have been identified within the IP gene that may predispose individuals to cardiovascular disease, including enhanced risk of deep vein thrombosis and intimal hyperplasia [22, 23].

The IP is primarily coupled to $G\alpha_s$ - adenylyl cyclase activation but may also regulate other effectors including Gq-mediated phospholipase (PL)Cβ activation, leading to phosphatidyl inositol turnover and mobilisation of calcium from intracellular stores [24-29]. The human (h)IP is subject to a number of co- and post-translational modifications that are critical to its function. Somewhat typical of other cell-surface GPCRs, it undergoes *N*-linked glycosylation, at Asn^7 and Asn^{78}, within its N-terminal and EC_1 domains, respectively, that influences its membrane localisation, ligand binding and signalling [30, 31]. Additionally, the hIP is somewhat unique among GPCRs in that it is both isoprenylated and palmitoylated within its C-tail domain. Farnesylation occurs in its distal C-tail domain at Cys^{383} within an evolutionary conserved –CAAX motif [32], while it is palmitoylated at three Cys residues (Cys^{308} , Cys^{309} and Cys^{311}) in the proximal C-tail adjacent to α-H8 (residues 297 – 307) of the hIP [33, 34]. Together, these dual lipidations are proposed to confer a double loop structure through the formation of a fourth (IC_4) and fifth (IC_5) IC loop within the C-tail of the hIP and are required to maintain G protein coupling and effector signalling [32, 33]. Furthermore, it has recently been established that both the mature, fully glycosylated (46 – 66 kDa) and immature, non-

glycosylated & core-glycosylated (38 – 44 kDa) species of the hIP may be polyubiquitinated and that this is required for lysosomal sorting of the mature, internalised receptors and for degradation of the immature species by the 26S proteasomes through the endoplasmic reticulum (ER)-associated degradation (ERAD) process, respectively [35].

Members of the Rab GTPases participate at multiple steps in the processing, maturation and intracellular trafficking of several GPCRs [36]. Most typically, Rab5a is present at the plasma membrane (PM) and early endosomes and mediates early endosome trafficking and fusion while Rab4a and Rab11a are associated with early and late recycling endosomes to regulate GPCR recycling through the so-called 'short' and 'long' recycling pathways, respectively [37-40]. Through recent studies, it has been established that the hIP undergoes agonist-induced internalisation through a Rab5a-dependent mechanism [41] and can be recycled to the PM through the 'slow' recycling path involving, somewhat unusually, a direct interaction between the hIP and Rab11a [42]. Indeed, the structural determinants required for its interaction with Rab11a have been determined and are localised to a 14-residue Rab11a binding domain (RBD) within the proximal C-tail domain of the hIP comprised of Val^{299} – Val^{307}, corresponding to much of its α-H8 domain, adjacent to the palmitoylation residues at Cys^{308} – Cys^{311} [34]. Furthermore, *Ala-scanning* mutagenesis of the 14-residue RBD revealed that hydrophobic residues, namely Phe^{300}, Leu^{303}, Leu^{305} and Val^{307}, which mainly lie on one face of the α-H8 were critical for the interaction with Rab11a. However, the fact that *Ala-scanning* mutagenesis of two positively charged residues, namely Arg^{302} and Lys^{304}, within α-H8 also disrupted the association between the hIP and Rab11a residues was inconclusive with regard to RBD function as the resultant mutated receptors (hIP^{R302A} and hIP^{K304A}) did not display a normal pattern of maturation or expression at the PM relative to the hIP itself [43].

Whilst the molecular basis for the failure of the hIP^{R302A} and hIP^{K304A} variants to mature and traffic to the PM was unclear, it was suggestive that these residues may possibly be part of an ER export motif most typically located within the proximal C-tail domain of many GPCRs [44, 45]. While many different or variant ER export motifs have been identified, perhaps the highly conserved $F(X)_6LL$ motif, proposed to be present in most, but not all, GPCRs, including the α_{1B}-adrenergic receptor (AR), α_{2B}-AR, β_2-AR and angiotensin II type 1A receptor (AT1R), is the most prevalent and widely characterized [46, 47]. Members of the prostanoid receptor subfamily, including the IP, are notable exceptions amongst GPCRs in that they do not contain the $F(X)_6LL$ motif [15]. Hence, the aim of the current study was to further investigate the molecular basis of the abnormal pattern of expression of the hIP^{R302A} and hIP^{K304A}, aiming to identify the major ER export motif within the hIP. Owing to the fact that *Ala-scanning* mutagenesis of the 14 residue RBD encompassing much of α-H8 revealed that mutation of Lys/Arg residues alone affected hIP expression led us to investigate whether other positively charged residues, such as within the C-tail domain of the hIP might also affect its maturation and/or expression at the PM. The hIP contains five Lys residues within its primary sequence where Lys^{218} is located in IC_3 while, notably, Lys^{297}, Lys^{304}, Lys^{342} and Lys^{376} are located in the C-tail domain (**Figure 1**). Hence, the initial aim was to investigate the role of Lys residues in the maturation and processing of the hIP and thereafter to define the ER export motif(s). Results herein identify a novel 8 amino acid ER export motif, $K/R(X)_4K/R(X)K/R$, within α-H8 of the hIP defined by a strict

requirement for three positively charged, basic Lys/Arg residues at the 1st, 6th and 8th positions, and represents a motif that is evolutionarily conserved in the IP sequences of many other species.

2.Materials & Methods

2.1 Materials

Cicaprost was a gift from Bayer Schering Pharma AG. [^{3}H]iloprost (15.3 Ci/mmol) was from Amersham Biosciences. Fura2/AM and epoxomicin were from Calbiochem. Fluo-4 was from Molecular Probes. QuikChange™ site-directed mutagenesis kit was from Stratagene. Effectene® transfection reagent was from Qiagen. The chemiluminescence western blotting kit and rat monoclonal 3F10 *anti*-HA antibody were from Roche. Mouse monoclonal *anti*-HA 101R antibody (1 mg/ml) was from Cambridge Biosciences. *Anti*-calnexin rabbit polyclonal antibody was from Bioquote. Horseradish peroxidase (HRP)-conjugated goat *anti*-rat IgG and goat *anti*-rabbit IgG antibodies were from Santa Cruz Biotechnology. AlexaFluor® 488 goat *anti*-rabbit IgG and AlexaFluor® 594 goat *anti*-mouse IgG were from Molecular Probes. DAPI and MG132 were obtained from Sigma. The oligonucleotides used in these studies were synthesised by Sigma-Genosys. The plasmid yellow fluorescent protein (YFP)-1,4-β-galactosyltransferase (YFP-β-Gal) [48] was a kind gift from Dr. Natalia Jura (Stony Brook University Cold Spring Harbor Laboratory, NY, U.S.A.).

2.2 Site-directed Mutagenesis of the hIP

The plasmid pHM6:hIP^{WT} has been previously described [49]. The plasmids pHM6:hIP^{K218Q}, pHM6:hIP^{K297Q}, pHM6:hIP^{K304Q}, pHM6:hIP^{K342Q}, pHM6:hIP^{K376Q}, pHM6:hIP^{K297,304Q}, pHM6:hIP^{K342,376Q}, pHM6:hIP^{K297,304,342Q}, pHM6:hIP^{K297,304,376Q}, pHM6:hIP^{K297,304,342,376Q}, pHM6:hIP^{K218,297,304,342,376Q}, pHM6:hIP^{K297A}, pHM6:hIP^{K304A}, pHM6:hIP^{K376A}, pHM6:hIP^{K297,304A}, pHM6:hIP^{A298G}, pHM6:hIP^{V299A}, pHM6:hIP^{F300A}, pHM6:hIP^{Q301A}, pHM6:hIP^{R302A}, pHM6:hIP^{L303A}, pHM6:hIP^{K297Q,R302L,K304Q}, pHM6:hIP^{K297R}, pHM6:hIP^{R302K}, pHM6:hIP^{K304R} and pHM6:hIP^{K297,304R} were generated using the template and sense/antisense primer pairs as outlined in **Table I**. Site-directed mutagenesis was performed using the QuikChange™ system (Stratagene) and all plasmids were validated using double-stranded DNA sequencing analysis.

2.3 Cell Culture and Establishment of Stable Cell Lines

Human embryonic kidney (HEK) 293 cells, obtained from the American Type Culture Collection, were cultured in minimum essential medium (MEM), supplemented with 10 % foetal bovine serum (FBS).

The HEK.hIP cell line stably overexpressing a HA-tagged form of the hIP has been previously described [49]. For the establishment of the other recombinant HEK 293 stable cell lines used herein, routinely, HEK 293 cells were plated at a density of 2 x 10^6 cells/100-mm dish approximately 48 hr prior to transfection. Cells were then transfected with 25 μg of *Pvu*I-linearised pHM6:hIP-based vector plus 10 μg of *Sca*I-linearised pAdVA [50] using the $CaCl_2$/DNA co-precipitation procedure, as previously described [51]. Forty-eight hours post-transfection, G418 (0.8 mg/ml) selection was applied. Individual G418-resistant colonies were selected after approximately 21 days and clonal cell lines were expanded giving rise to the HEK.hIP-based cell lines. Expression of the hIP in these stable cell lines was assayed by radioligand-binding assays, as outlined below.

2.4 Radioligand-binding Assays

Radioligand-binding assays (RLBAs) of the IP were carried out as previously described [52]. Briefly, cells were harvested by centrifugation at 500 x *g* at 4 °C for 5 min and washed three times with ice-cold PBS. Following resuspension in Homogenisation Buffer (25 mM Tris/HCl, pH 7.5; 0.25 M sucrose; 10 mM $MgCl_2$; 1 mM EDTA; 0.1 mM phenylmethylsulfonyl fluoride (PMSF)), cells were homogenised and centrifuged at 100,000 x *g* for 60 min at 4 °C. The pellet fractions (P_{100}), representing crude membranes, were resuspended in Resuspension Buffer (10 mM MES/KOH, pH 6.0; 10 mM $MnCl_2$; 1 mM EDTA; 10 mM indomethacin). Protein determinations were carried out using the Bradford assay [53]. RLBAs were carried out at 30 °C for 1 hr in a final assay volume of 100 µl using 35 - 100 µg of membrane P_{100} fraction/assay in the presence of 4 nM [^{3}H]iloprost (15.3 Ci/mmol), for saturation binding studies, or in the presence of 0.1–200 nM [^{3}H]iloprost for Scatchard analysis. Nonspecific binding was determined in the presence of 0.2 mM iloprost for saturation binding studies or in the presence of 500-fold molar excess of nonlabeled iloprost for Scatchard binding studies. Alternatively to analyse cell surface IP expression, following harvesting and washing in PBS, cells were resuspended in MES/KOH buffer and RLBAs were carried out at 4 °C for 1 hr, using 35 - 100 µg of whole cell protein in 100 µl reactions in the presence of 4 nM [^{3}H]iloprost (15.3 Ci/mmol) as previously described. Reactions were terminated by the addition of 4 ml of ice-cold Resuspension Buffer followed by filtration through Whatman GF/C filters, which had been pretreated in 0.3 % polyethyleneimine (PEI) for 1 – 24 hr. The filters were washed three times with Resuspension Buffer (4 ml) and radioactivity counted in scintillation fluid (5 ml/filter) using a Tri-Carb 2900TR Liquid Scintillation Analyzer. Radioligand binding data were analyzed using the PRISM 5 computer program (GraphPad Software Inc., San Diego, CA) to determine the K_d and B_{max} values. The suitability of both one-site and two-site binding models was examined using the F-test. The level of significance of the results of the F-test were tested to $p < 0.05$.

2.5 Measurement of Intracellular Ca^{2+} Mobilisation

Measurement of intracellular Ca^{2+} ($[Ca^{2+}]_i$) mobilisation in Fura2/AM-preloaded cells was carried out essentially as previously described [51]. Briefly, cells were harvested and washed three times in ice-cold PBS. Cells were resuspended (1.6 x 10^6 cells/ml) in modified Ca^{2+}/Mg^{2+}-free HBSSHB (Hanks' buffered salt solution containing 20 mM HEPES, pH 7.67, 0.1 % bovine serum albumin (BSA)) and were loaded with 5 µM Fura2/AM for 40 min at 37 °C in the dark. Thereafter, cells were harvested by centrifugation at 500 x *g* for 5 min at room temperature (RT), washed once in HBSSHB and finally diluted to 0.8 x 10^6 cells/ml in HBSSHB containing 1 mM $CaCl_2$. Cells (2 ml aliquots) were then stimulated with cicaprost (1 µM) and Fura2 fluorescence from gently stirred cells was recorded using a Perkin-Elmer LS50-B spectrofluorometer at excitation wavelengths of 340 nM and 380 nM and an emission wavelength of 510 nm [54]. Alternatively, for determination of half maximal effective concentration (EC_{50}) values, cells were harvested and washed thrice in Krebs/HEPES buffer (118 mM NaCl, 4.7 mM KCl, 1.2 mM $MgSO_4$, 1.2 mM KH_2PO_4, 4.2 mM $NaHCO_3$, 11.7 mM D-glucose, 1.3 mM $CaCl_2$, 10 mM HEPES, pH 7.4) prior to pre-loading with Fluo-4/AM (1 hr at 25 °C; 3 µM in Krebs/HEPES buffer containing 1% Pluoronic F-127). Thereafter, cells

were washed twice and resuspended (3 x 10^5 cells/ml) in Krebs/HEPES buffer containing 0.5 % BSA. Cells (0.18 ml aliquots) were then stimulated with cicaprost (0.01 nM - 5 μM) and Fluo-4 fluorescence was recorded using a Fluoroskan Ascent microplate fluorometer at excitation wavelength of 485 nM and an emission wavelength of 518 nm [55]. For each $[Ca^{2+}]_i$ mobilisation, calibration of the fluorescence signal was performed in 0.2 % Triton X-100 to obtain the maximal fluorescence (R_{max}) and in 1 mM EGTA, to obtain the minimal fluorescence (R_{min}). The ratio of the fluorescence at 340 nM to that at 380 nM in Fura2-loaded cells or fluorescence at 518 nm in Fluo-4-preloaded cells is a measure of $[Ca^{2+}]_i$ mobilisation, assuming a K_d of 225 nM or 345 nM Ca^{2+} for Fura2/AM or Fluo-4, respectively. Data presented are representative of at least three independent experiments and were calculated as mean changes in intracellular Ca^{2+} mobilised ($\Delta[Ca^{2+}]_i \pm$ S.E.M., nM) as a function of time (s) following ligand stimulation.

2.6 Immunoprecipitations, SDS-PAGE and Western Blotting.

To examine expression of the HEK.hIP-based stable cell lines, cells were seeded at 2 x 10^5 cells/well in 6-well plates and grown for 72 – 96 hr. Thereafter, cells were harvested in 1 X PBS, pH 7.4 containing protease inhibitors (0.5 mM PMSF; 2.0 mM 1, 10 phenanthroline; 10 μg/ml aprotinin; 1 mM benzamidine hydrochloride; 1 μg/ml leupeptin). In order to examine the effect of the proteasomal inhibition on hIP expression, cells were incubated with MG132 (10 μM), epoxomicin (0.1 μM) or, as control, with vehicle (0.001% DMSO) for 12 hr. In all cases, protein concentration was assayed using the Bradford assay [53]. Generally, 50 μg total cellular protein was resuspended in SDS-sample Buffer (10 % β-mercaptoethanol (v/v); 2 % SDS (w/v); 30 % glycerol (v/v); 50 mM Tris-HCl, pH 6.8; 0.025 % bromophenol blue (w/v)). Samples were then boiled for 10 min prior to resolution by SDS-PAGE, on 10 % polyacrylamide gels, followed by electroblotting onto PVDF membrane. Blots were screened versus the *anti*-HA (3F10; 1:1,000) antibody, followed by the secondary HRP-conjugated goat *anti*-rat IgG antibody (1:5,000), and HA-tagged proteins were visualised using the chemiluminescence detection system, as described by the supplier. All blots illustrated in the figures are representative blots from 3 – 6 experiments (n = 3 – 6).

In order to examine the possible interaction of the ER chaperone protein calnexin with the hIP, following harvesting and washing, cells were lysed in radio-immunoprecipitation (RIP) Buffer (50 mM Tris-HCl, pH 8.0, 150 mM NaCl, 1 mM EDTA, 1% NP-40 (v/v), 0.5% sodium deoxycholate (w/v), 0.1% SDS (w/v), 10 mM sodium fluoride, 25 mM sodium pyrophosphate) supplemented with protease inhibitors (1 mM PMSF; 10 μg/ml aprotinin; 1 μg/ml leupeptin) and lysed by sequentially passing through hypodermic needles of decreasing bore size (18-, 21-, 23- and 26-gauge), as previously described [35]. HA-tagged receptors from resulting supernatants (~600 μg) were immunoprecipitated with *anti*-HA (101R; 1 in 300) antibody at 4 °C for 16 hr, processed and analysed by SDS-PAGE, on 10 % acrylamide gels, and western blotting essentially as previously described [43]. Blots were screened using the *anti*-calnexin and *anti*-HA (3F10) antisera followed by chemiluminescence detection.

2.7 Confocal Microscopy

HEK.hIP-based cells were seeded onto coverslips, which were pretreated with 0.1 mg/ml poly-L-lysine in 6-well plates, and grown for 48 hr. Where indicated, cells were transiently transfected with the plasmid YFP-β-Gal encoding the Golgi marker or, as control, with empty vector using Effectene® transfection reagent, essentially as outlined by the manufacturer (Qiagen). Forty-eight hr post-transfection, cells were fixed using 3.7 % paraformaldehyde, 1 X PBS, pH 7.4, for 15 min at RT and thereafter washed three times with PBS. Cells were permeabilised by incubation with 0.2 % Triton X-100 in PBS for 10 min on ice, followed by washing with 1 X TBS. Nonspecific sites were blocked by incubating cells with 1 % BSA, 1 X TBS, pH 7.4 for 1 hr at RT. Cells were incubated with either the *anti*-HA 101R primary antibody (1:1,000 in 1 % BSA) to label the HA-tagged hIP receptors or the *anti*-calnexin primary antibody (1:150 in 1 % BSA) to label the ER for 1 hr at RT. The antibody solution was removed and cells were washed twice with 1 X TBS followed by further incubation with 1 % BSA for 30 min. Cells were then incubated with Alexa Fluor® 594 goat *anti*-mouse IgG secondary antibody (1:4,000 in 1 % BSA) to detect the HA-tagged receptors and/or Alexa Fluor® 488 goat *anti*-rabbit IgG secondary antibody (1:4,000 in 1 % BSA) to detect the ER for 1 hr at RT. Cells were washed twice in 1 X TBS prior to counterstaining of the nuclei with DAPI (1 μg/ml in H_2O). Coverslips were mounted onto glass slides using fluorescent mounting medium (Dako). Slides were then imaged at x63 magnification using a Carl Zeiss Lazer Scanning System LSM510 and Zeiss LSM Imaging software.

2.8 Computational Structure Predictions

Structure prediction of the hIP, consistent with a previous report [43], and of the variant $hIP^{K297Q,R302L,K304Q}$ or of the human β_1 adrenergic receptor (h.β_1AR; NP_000675) were generated by online submission to the iterative TASSER (I-TASSER) algorithm, a three dimensional structure prediction software that builds models based on multiple-threading consensus target-to-template alignments by LOM-ETS (Local Meta-Threading Server) and I-TASSER simulations (available on the University of Michigan web site) [56, 57]. I-TASSER predictions were in agreement with those generated from independent predictions using PHYRE (available on the World Wide Web) and were further analysed for helical content using the AGADIR prediction algorithm (available on the World Wide Web). Amphipathic helical predictions were carried out using the online tool (available on the World Wide Web). Jpred 3 [58], a web system of different secondary structure prediction algorithms (see the University of Dundee web site) was used to confirm that mutations generated, such as by the *Ala-scanning* mutagenesis, *per se* did not affect the formation of the α-H8 domain.

2.9 Data Analyses

Statistical analyses were carried out using the unpaired Student's *t*-test or, where relevant and specifically indicated in the text, using two-way ANOVA employing the GraphPad Prism package. *P*-values of ≤ 0.05 were considered to indicate a statistically significant difference.

3. Results

3.1 Role of Lysines in Influencing the Expression and Intracellular Signalling of the hIP

The human prostacyclin receptor (hIP) contains five Lys residues where Lys^{218} is located in IC_3 and the remaining 4 (Lys^{297}, Lys^{304}, Lys^{342} and Lys^{376}) are located in its C-tail domain (**Figure 1**). Hence, the initial aim was to investigate the role of Lys residues in the maturation and processing of the hIP. To this end, each of the five Lys residues were mutated, either individually or in various combinations, by semi-conservative substitution to corresponding Gln (Q) residues, thereby minimising any potential non-specific mutational effects. In all, cDNAs encoding 11 different '*Lys to Gln'* variants of the hIP were generated (**Table I**) and clonal cell lines stably over-expressing hemagglutinin (HA)-tagged forms of each receptor were established in mammalian human embryonic kidney (HEK) 293 cells. Those stable cell lines were characterised by western blot analysis to assess receptor expression levels and, functionally, by radioligand binding assays (RLBAs) and by assessment of agonist-induced intracellular calcium ($[Ca^{2+}]_i$) mobilisation, where data throughout was compared to the previously characterised HEK.hIP cell line expressing a HA-tagged form of the wild type hIP [49].

Consistent with a previous report [35], western blot analysis of whole cell protein from HEK.hIP cells showed that the hIP is predominantly expressed as a mature, fully glycosylated species (46 – 66 kDa) and as an immature, core glycosylated, non-farnesylated intermediate species detected at ~ 44 kDa (**Figure 2A**) while the lesser abundant immature, core glycosylated, farnesylated intermediate species, detected at ~ 42 kDa, is only evident following prolonged exposure of the immunoblots (data not shown). No expression of HA-tagged protein was detected in the control HEK 293 cell line (**Figure 2A**). The overall pattern of expression of hIP^{K218Q} and hIP^{K376Q} was, in effect, identical to that of the wild-type hIP (**Figure 2A**). While the hIP^{K342Q} and $hIP^{K342,376Q}$ (**Figure 2A**) showed significant expression of both core glycosylated intermediates (44 and 42 kDa) and the fully mature, glycosylated species (46 – 66 kDa), their overall migration patterns were somewhat slower than those of the hIP and hIP^{K376Q}. The reason for this altered migration is unknown, but suggests that mutation of Lys^{342} alters the pattern of glycosylation of the hIP. In the case of the hIP^{K297Q} and hIP^{K304Q}, both of these receptor variants were almost exclusively expressed as the immature core glycosylated intermediate (44 kDa), while the levels of their mature, fully glycosylated species were barely detectable (**Figure 2A,** compare hIP^{K297Q} and hIP^{K304Q} to the hIP). Longer exposure of the immunoblot was required to detect the 42 kDa species (data not shown). Analysis of whole cell protein from HEK.$hIP^{K297,304Q}$ cells (**Figure 2A**) also demonstrated that the $hIP^{K297,304Q}$ is predominantly expressed as the core glycosylated 44 and 42 kDa intermediates with almost a complete absence of the mature, fully glycosylated species. Additionally, and consistent with this, the $hIP^{K297,304,342Q}$, $hIP^{K297,304,376Q}$, $hIP^{K297,304,342,376Q}$ and $hIP^{K218,297,304,342,376Q}$ were also predominantly expressed as the core glycosylated 44 and 42 kDa intermediates (**Figure 2A**). Therefore, the presence of Lys^{297} and/or Lys^{304} appears to be essential for complete glycosylation and maturation of the hIP.

RLBAs, using crude (P_{100}) membrane fractions and employing [^{3}H]iloprost as selective radioligand, established that the level of hIP expression in HEK.hIP cells was typically 1.55 ± 0.25 pmol/mg membrane protein (**Figure 2B**). There was no significant difference in [^{3}H]iloprost binding by the hIP^{K218Q}, hIP^{K342Q},

hIP^{K376Q} or $hIP^{K342,376Q}$ receptors relative to that of the wild-type hIP (**Figure 2B**). However, radioligand binding by the hIP^{K297Q} and hIP^{K304Q} were reduced by 74.8 % and 54.2 %, respectively, compared to the hIP (**Figure 2B**, $p < 0.01$ & $p < 0.05$, respectively), while that of $hIP^{K297,304Q}$ was reduced by 83.9 % (**Figure 2B**, $p < 0.01$). Additionally, [^{3}H]iloprost binding by the $hIP^{K297,304,342Q}$, $hIP^{K297,304,376Q}$, $hIP^{K297,304,342,376Q}$ and $hIP^{K218,297,304,342,376Q}$ were significantly reduced compared to the hIP (**Figure 2B**, $p < 0.01$ in each case). **Collectively**, RLBA data confirmed that all variant hIPs carrying the *'Lys^{297} to Gln^{297}'* or *'Lys^{304} to Gln^{304}'* mutations, either alone or in combination with any of the other *'Lys to Gln'* mutations displayed impaired [^{3}H]iloprost binding relative to the wild-type hIP and correlated well with observations from western blotting data (**Figure 2A**).

In order to assess whether the alteration in ligand binding by the *'Lys^{297} to Gln^{297}'* or *'Lys^{304} to Gln^{304}'* variants is actually due to alterations in receptor expression at the cell surface, RLBAs were also carried out on whole cells by incubation with [^{3}H]iloprost at 4 °C. Consistent with previous studies [33], incubation with [^{3}H]Iloprost at 4 °C, as opposed to at 30 °C, inhibits agonist-induced internalization of the hIP, allowing for more accurate measurement of the cell surface expression of the hIP using whole cells as opposed to using crude membrane preparations present in P_{100} fractions. Using this approach, levels of hIP expression in HEK.hIP cells were typically 1.93 ± 0.06 pmol/mg whole cell protein (**Figure 2C**) and there was no substantial difference in the level of expression of the hIP^{K218Q}, hIP^{K342Q} or hIP^{K376Q} at the cell surface relative to the hIP. In contrast, expression of both the hIP^{K297Q} and hIP^{K304Q} were reduced by 69.9 % and 62.7 %, respectively, compared to the hIP (**Figure 2C**, $p < 0.05$ in each case), while that of $hIP^{K297,304Q}$ was reduced by 90.3 % (**Figure 2C**, $p < 0.005$). Moreover, Scatchard analyses determined that while there were no substantial differences in the affinity constant (*Kd*) at either the high or low affinity binding sites of any of the *'Lys to Gln'* variants studied (**Table 2**). However, consistent with the saturation radioligand binding data (Figure 2B & 2C), there was substantial variations in the Bmax values in variants carrying *Lys^{297} to Gln^{297}'* or *'Lys^{304} to Gln^{304}'* mutations at both the high and low affinity binding sites but at levels entirely reflective of those in Figure 2B & 2C (data not shown).

The consequence of the *'Lys to Gln'* mutations on functional hIP expression was also examined by analysis of agonist-induced $[Ca^{2+}]_i$ mobilisation in response to stimulation of the HEK 293 clonal cell lines with the highly selective IP agonist cicaprost. Stimulation of HEK.hIP cells generated a large transient rise in $[Ca^{2+}]_i$ mobilisation in response to cicaprost which was significantly greater than that of the control HEK 293 cell line (**Figure 2D**; compare 20.1 ± 3.7 nM versus 141.2 ± 5.8 nM, $p < 0.001$). Levels of $[Ca^{2+}]_i$ mobilised by the hIP^{K218Q}, hIP^{K342Q}, hIP^{K376Q} or $hIP^{K342,376Q}$ were not significantly different to the hIP (**Figure 2D**). Hence, while the hIP^{K342Q} and $hIP^{K342,376Q}$ exhibit slightly modified patterns of glycosylation compared to wild-type hIP, this does not affect their ability to bind radioligand or to mobilise $[Ca^{2+}]_i$ in response to agonist-stimulation. In contrast, levels of $[Ca^{2+}]_i$ mobilisation by the hIP^{K297Q} and hIP^{K304Q} were reduced by 62.7 % and 44.4 %, respectively, compared to the hIP (**Figure 2D**, $p < 0.001$ & $p < 0.01$, respectively). Furthermore, levels of cicaprost-induced $[Ca^{2+}]_i$ mobilisation by the $hIP^{K297,304Q}$, $hIP^{K297,304,342Q}$, $hIP^{K297,304,376Q}$, $hIP^{K297,304,342,376Q}$ and $hIP^{K218,297,304,342,376Q}$ were reduced by 52.1 %, 54.3 %, 49.4 %, 61.5 % and 68.8 %, respectively, compared to the hIP (**Figure 2D**, $p < 0.001$ in each case). Furthermore, despite

such differences in overall levels of $[Ca^{2+}]_i$ mobilised, concentration -response studies established that EC_{50} values for cicaprost-induced $[Ca^{2+}]_i$ mobilisation by any of the '*Lys to Gln'* variants studied were not substantially different to that of the wild type hIP, including those variants carrying the *'Lys^{297} to Gln^{297}'* or *'Lys^{304} to Gln^{304}'*, either alone or in combination with other mutated Lys residues (**Table 3**). More specifically, those EC_{50} values ranged between ~10 – 30 nM and any variations from that of the wild type hIP were not exclusively attributable to those variants carrying the *'Lys^{297} to Gln^{297}'* or *'Lys^{304} to Gln^{304}* (**Table 3**). Collectively, these data correlate well with previous western blotting and RLBA data and confirm that all hIP variants carrying the *'Lys^{297} to Gln^{297}'* or *'Lys^{304} to Gln^{304}'* mutations, either alone or in any combination, are functionally defective whereby they do not efficiently traffic to the plasma membrane (PM) and display substantially reduced ligand binding and agonist-induced $[Ca^{2+}]_i$ mobilisation (**Figure 2A – 2D**).

The significant reductions in the relative expression of the 46 – 66 kDa species of the hIP variants carrying the *'Lys^{297} to Gln^{297}'* or *'Lys^{304} to Gln^{304}'* mutations, coupled to their diminished functional expression suggested that those receptors had impaired maturation to their fully glycosylated forms and/or were unable to efficiently traffic to the PM. Hence, confocal image analysis was used to investigate the subcellular localisation of the hIP and each of the *'Lys to Gln'* variants expressed in the respective clonal cell lines (**Figure 2E**). More specifically, it was sought to investigate whether the maturation and/or intracellular trafficking of the hIP^{K297Q}, hIP^{K304Q} and hIP^{K218,297,304,342,376Q} may be disrupted, resulting in their accumulation in the ER and/or the Golgi complex. To locate the ER, cells were stained with an antibody directed to the ER marker protein calnexin. The ER appears as a dense, reticular network in HEK 293 cells, with particularly strong staining around the nuclear envelope. To locate the Golgi, cells were cotransfected with an expression plasmid encoding YFP-β-gal, a recombinant Golgi-complex marker protein encoding the yellow-green variant of *Aequorea victoria* green fluorescent protein fused to the trans-medial Golgi membrane-anchoring signal peptide of human β-1,4-galactosyltransferase [48].

The HA-tagged hIP was mainly expressed at the PM in HEK.hIP cells with relatively little intracellular localisation (**Figure 2E,** *Anti*-HA) and no colocalisation with either calnexin or YFP-β-gal apparent in these cells (**Figure 2E,** *Anti*-Calnexin, YFP-β-gal and Overlay panels). Consistent with this, each of the single hIP^{K218Q}, hIP^{K342Q}, hIP^{K376Q} and double hIP^{K342,376Q} mutated receptors, which bound radioligand and mobilised $[Ca^{2+}]_i$ in a manner similar to the wild-type hIP, were mainly expressed at the PM and did not colocalise with the ER or Golgi markers (**Figure 2E**), data is presented for HEK.hIP^{K218Q} and HEK.hIP^{K342,376Q} cells only). In contrast, the staining pattern detected in cells expressing the hIP^{K297Q}, hIP^{K304Q}, hIP^{K297,304Q}, hIP^{K297,304,342Q}, hIP^{K297,304,376Q}, hIP^{K297,304,342,376Q} and hIP^{K218,297,304,342,376Q} receptors was significantly different from the wild-type hIP (**Figure 2E**), where data is presented for HEK.hIP^{K297Q}, HEK.hIP^{K304Q} & HEK.hIP^{K218,297,304,342,376Q} cells only). Both hIP^{K297Q} and hIP^{K304Q} exhibited very poor expression at the PM, mainly showing a diffuse cytoplasmic staining (**Figure 2E**, *Anti*-HA). Furthermore, both the hIP^{K297Q} and hIP^{K304Q} strongly colocalised with the ER marker calnexin, but not with the Golgi marker YFP-β-Gal (**Figure 2E**, Overlay). In certain cell fields, a small fraction of the cellular pool of the hIP^{K297Q} and hIP^{K304Q} were capable of trafficking to the PM (for example, see **Figure 2E**, *Anti*-HA). This correlated well with western blotting data which indicated that a small proportion of the hIP^{K297Q} and

hIP^{K304Q} were detected as the fully glycosylated, mature species (**Figure 2A**). In the case of the hIP^{K218,297,304,342,376Q}, devoid of all Lys residues, it was unable to traffic to the PM (**Figure 2E**, *Anti*-HA), and showed strong co-localisation with calnexin but not with YFP-β-Gal. Moreover, the hIP^{K218,297,304,342,376Q} strongly colocalised with the ER, but not with the Golgi complex marker (**Figure 2E**, Overlay panels). Combined, these data suggest that any variant hIPs possessing either the '*Lys^{297} to Gln^{297}*' or '*Lys^{304} to Gln^{304}*' mutations, either alone or in any combination, were not expressed at or exported to the PM, being retained in the ER compartment of the cell. Therefore, mutation of Lys^{297} and/or Lys^{304} disrupts the normal anterograde transport of the hIP from its site of synthesis in the ER through to the Golgi complex, where final post-translational modification including end-stage glycosylation occurs, before the receptor is transported to its functional site at the PM.

3.2 Investigation of the Turnover of the hIP through ERAD and Interaction with the ER Chaperone Calnexin.

As previously stated, we have recently established that immature species of the hIP are degraded through ERAD involving the ubiquitin-dependent 26S proteasomal pathway while turnover of the mature, fully glycosylated receptor mainly occurs through the lysosomal pathway [35]. While the observed effects resulting from the mutational studies herein of *'Lys^{297} to Gln^{297}'* or *'Lys^{304} to Gln^{304}'*, either alone or in combination with the other Lys^{218}, Lys^{342} or Lys^{376} residues, may occur due to disruption of residues within a putative ER export motif(s), another explanation may be that they occur either due to (i) increased degradation of their immature forms through ERAD and/or (ii) their misfolding due to altered association with ER resident chaperone proteins such as calnexin. Hence, to address the first of these possibilities, (i) we examined the effect of the 26S proteasomal inhibitors MG132 and/or epoxomicin on the expression of the hIP and of its variants carrying the *'Lys^{297} to Gln^{297}'* or *'Lys^{304} to Gln^{304}'* mutations (**Figure 3A & Supplemental Figure S1**). Consistent with previous reports [35], preincubation of HEK.hIP cells with MG132 and/or epoxomicin led to accumulation of 4 immature species of the hIP (38 – 44 kDa) but had no effect on the level of expression of the fully glycosylated mature species (~ 44-66 kDa; **Figure 3A & Supplemental Figure S1**). Similarly, preincubation of cells expressing either the hIP^{K297Q}, hIP^{K304Q}, hIP^{K297,304Q} and hIP^{K218,297,304,342,376Q}, which are each exclusively expressed as the core glycosylated 44 and 42 kDa intermediates with almost a complete absence of the mature, fully glycosylated species, with MG132 and/or epoxomicin also led to accumulation of the 4 immature species of the hIP (38 – 44 kDa) and at levels similar to those of the wild type hIP (**Figure 3A & Supplemental Figure S1**). Hence, these data are consistent with the previous study that established that the hIP is subject to degradation through the ERAD system [35] and, more specifically, that this occurs irrespective of whether it is the wild type hIP or mutated variants containing the K^{297Q} or K^{304Q} mutations.

To address the possibility that the hIP variants carrying the *'Lys^{297} to Gln^{297}'* or *'Lys^{304} to Gln^{304}'*, either alone or in combination with the other Lys^{218}, Lys^{342} or Lys^{376} residues, may display reduced trafficking and functional expression at the PM due to (ii) possible altered association with ER chaperones, the interaction of the hIP and '*Lys to Gln*' variants with endogenous calnexin was investigated through co-

immunoprecipitation studies (**Figure 3B**). Calnexin was associated with each of the *anti*-HA immunoprecipitates from the respective clonal HEK 293 cells over-expressing HA- tagged forms of the hIP^{WT}, hIP^{K218Q}, hIP^{K297Q}, hIP^{K304Q}, hIP^{K342Q}, hIP^{K376Q} and $hIP^{K218,K297,K304,K342,K376Q}$ but was not present in corresponding *anti*-HA immune complexes from the control HEK 293 cells (**Figure 3B**). Hence, collectively, these data establish that the effects of the "*Lys to Gln*" mutations are not due to alterations in their degradation through ERAD or in their folding status *per se* relative to that of the wild type hIP but rather, more specifically, are consistent with the suggestion that the *'Lys^{297} to Gln^{297}'* or *'Lys^{304} to Gln^{304}'*mutations disrupt a putative ER export motif within the hIP.

3.3 Effect of Mutation of *'Lys^{297} to Ala^{297}'* and *'Lys^{304} to Ala^{304}'* on Expression, Intracellular Signalling and Subcellular Localisation of the hIP

To exclude the possibility that the observed altered maturation and functional expression of the hIP^{K297Q} and hIP^{K304Q} may be an artefact of the choice of '*Lys^{297} to Gln^{297}*' or '*Lys^{304} to Gln^{304}*' substitutions, additional mutational analysis was carried out whereby Lys^{297} and Lys^{304} were mutated, either individually or in combination, to corresponding Ala residues, with subsequent characterisation of the respective clonal HEK 293 cell lines (**Table 1 & Figure 4**), as previous. As an additional control for these studies, the consequence of mutation of Lys^{376} to Ala^{376} by generating the hIP^{K376A} variant was also investigated.

The hIP and the hIP^{K376A} were expressed as the mature, fully glycosylated species (46 – 66 kDa), with the core glycosylated intermediate species detected at ~ 44 kDa and 42 kDa (**Figure 4A**). The hIP^{K297A}, hIP^{K304A} and $hIP^{K297,304A}$ were almost exclusively expressed as the core glycosylated intermediates (44 and 42 kDa), with very little expression of the mature, fully glycosylated receptors in any case (**Figure 4A**). This pattern of protein expression by hIP^{K297A}, hIP^{K304A} and $hIP^{K297,304A}$ was, in effect, identical to that of hIP^{K297Q}, hIP^{K304Q} and $hIP^{K297,304Q}$ (**Figure 2A**), thereby verifying that the lack of mature, fully glycosylated species associated with mutation of either Lys^{297} or Lys^{304} residues was not an artefact of the nature of the mutation, be it a Gln or Ala, *per se*.

Assessment of [^{3}H]iloprost binding confirmed that radioligand binding by the hIP^{K297A}, hIP^{K304A} and $hIP^{K297,304A}$ was significantly impaired (**Figure 4B,** $p < 0.01$), while that of the control hIP^{K376A} was almost identical to the wild type hIP. Furthermore, consistent with their reduced cell surface expression, cicaprost-induced $[Ca^{2+}]_i$ mobilisation by hIP^{K297A}, hIP^{K304A} and $hIP^{K297,304A}$, but not that by the hIP^{K376A}, was significantly reduced compared to the hIP (**Figure 4C**, $p < 0.001$). Analysis of the subcellular distribution by immunofluorescence microscopy revealed that while the hIP and hIP^{K376A} were each mainly expressed at the PM and did not co-localise with calnexin (**Figure 4D**), the hIP^{K297A}, hIP^{K304A} and $hIP^{K297,304A}$ showed intracellular expression, with marked colocalisation with the ER marker calnexin (**Figure 4D**). The lack of cell surface expression of hIP^{K297A}, hIP^{K304A} and $hIP^{K297,304A}$ is consistent with the previous imaging data for the '*Lys^{297} to Gln^{297}*' or '*Lys^{304} to Gln^{304}*' substitutions (**Figure 2E**). Therefore, these data confirm that mutation of Lys^{297} and/or Lys^{304} to corresponding Gln or Ala residues results in the failure of the hIP to be exported from the ER to the Golgi complex and to undergo full end-stage glycosylation and maturation with subsequent expression at the PM.

3.4 *Ala-scanning* Mutagenesis of Lys^{297} - Lys^{304} to Identify Critical Residues Required for the Export of the hIP from the ER

Lys^{297} and Lys^{304}, established as key residues required for the transport of the hIP from the ER to the PM (**Figures 2 & 4**), are located within α-H8 of the hIP, the domain located within its proximal C-tail and predicted to span Lys^{297} – Val^{307} adjacent to the palmitoylated Cys^{308} – Cys^{311} residues (**Figure 1**). In order to determine if any other residues within α-H8 may be required for the cell surface expression and/or maturation of the hIP, *Ala-scanning* mutagenesis was performed whereby each residue from Lys^{297} – Lys^{304} was individually substituted with Ala, except in the case of Ala^{298} which was mutated to the alternative neutral residue Gly^{298} in that position (**Figure 5A**).

Similar to the wild-type hIP, hIP^{A298G}, hIP^{V299A}, hIP^{F300A}, hIP^{Q301A} and hIP^{L303A} were each expressed in their respective clonal HEK 293 stable cell lines as the mature, fully glycosylated species (46 – 66 kDa) and as the core glycosylated intermediate species at ~ 44 kDa and 42 kDa (**Figure 5B**). The migration pattern of the mature species of hIP^{L303A} (**Figure 5B**) was somewhat faster than that of the hIP, suggesting that mutation of Leu^{303} may alter the pattern of glycosylation of the hIP. Consistent with previous data (**Figure 4A**), hIP^{K297A} and hIP^{K304A} were mainly expressed as the core glycosylated intermediate species (**Figure 5B**). Strikingly, the hIP^{R302A} was also mainly expressed as the immature core glycosylated intermediates, with very limited expression of the mature 46 – 66 kDa species evident (**Figure 5B**). These data suggest that Arg^{302}, in addition to Lys^{297} and Lys^{304}, was absolutely required for complete glycosylation and maturation of the hIP.

Levels of [^{3}H]iloprost binding and cicaprost-induced $[Ca^{2+}]_i$ mobilisation by hIP^{A298G}, hIP^{V299A}, hIP^{F300A}, hIP^{Q301A} and hIP^{L303A} were modestly reduced in comparison to that of the hIP, but these reductions were not found to be significant (**Figure 5C & 5D**). On the other hand, and consistent with western blot analysis (**Figure 5B**) and previous data (**Figure 4**), both [^{3}H]iloprost binding and cicaprost-induced $[Ca^{2+}]_i$ mobilisation by hIP^{K297A}, hIP^{R302A} and hIP^{K304A} cells were significantly reduced compared to the hIP (**Figure 5C**, $p < 0.01$ & **Figure 5D**, $p < 0.001$, respectively). Moreover, confocal imaging confirmed that, similar to the wild type hIP, each of the hIP^{A298G}, hIP^{V299A}, hIP^{F300A}, hIP^{Q301A} or hIP^{L303A} were mainly expressed at the PM (data not shown). Conversely, the hIP^{R302A} (**Figure 5E**) displayed a similar pattern of expression to that of hIP^{K297Q}, hIP^{K304Q}, hIP^{K297A} or hIP^{K304A} (**Figures 2E & 4D**) in that it was not expressed at the PM but rather exhibited diffuse intracellular staining and extensive co-localisation with calnexin (**Figure 5E**). Collectively, these data suggest that Lys^{297}, Arg^{302} and Lys^{304} are specifically required for the export of the hIP from the ER and subsequent maturation and trafficking to the PM.

3.5 Effect of Introducing the 'F(X)$_6$LL' ER Export Motif on Expression and Signalling by $hIP^{K297,304Q}$

The sequence 'F(X)$_6$LL', where F is Phe, X is any amino acid and L is Leu or Ile, has been identified as an ER export motif located within the proximal C-tail domains of many GPCRs including that of the α_{2B}-AR, β_1-AR and AT1R [46, 47]. While this somewhat canonical F(X)$_6$LL motif is not found in the primary sequence of any of the 8 members of the prostanoid receptor subfamily of GPCRs, including of the hIP,

alignment of the sequences of the hIP and the β_1-AR reveals a marked similarity in this region except that the critical diLeu of the 'F(X)$_6$LL' is not present in the hIP (**Figure 6A**). Data presented in the current study established that mutation of the critical Lys^{297} and Lys^{304} to corresponding Gln residues generated the hIP^{K297,304Q} that was retained in the ER, failing to mature into a functional receptor located at the PM (**Figure 2**). Therefore, herein, it was sought to investigate whether introduction of the F(X)$_6$LL motif into the hIP^{K297,304Q} by simple substitution of Arg^{302} to Leu^{302} would rescue its defect and allow for export of the resulting hIP^{K297Q,R302L,K304Q} from the ER, facilitating its maturation and functional expression at the PM. Noteworthy, molecular modelling using I-TASSER simulations confirmed that the F(X)$_6$LL motif within both the human β_1AR **(Figure 6B (i))** and the hIP^{K297Q,R302L,K304Q} **(Figure 6B (ii))** are located in almost the same positions, namely predominantly within their corresponding α-H8 domains in the membrane proximal region of their C-tail domains.

Hence, site-directed mutagenesis was employed to mutate Arg^{302} to Lys^{302} in the hIP^{K297,304Q} and the resulting cDNA was stably transfected into HEK 293 cells to generate the HEK.hIP^{K297Q,R302L,K304Q} cell line (**Figure 6**). Analysis of whole cell protein by western blotting revealed that, unlike the hIP, the pattern of expression of the hIP^{K297Q,R302L,K304Q} was similar to the hIP^{K297,304Q}, whereby it was mainly expressed as the core glycosylated intermediate species (~ 44 and 42 kDa) but the mature, fully glycosylated species (46 – 66 kDa) were absent (**Figure 6C,** compare hIP^{K297Q,R302L,K304Q} & hIP^{K297,304Q}). The lack of mature species of the hIP^{K297Q,R302L,K304Q} was further confirmed by the fact that both [^{3}H]iloprost binding (**Figure 6D**, $p < 0.01$) and cicaprost-induced $[Ca^{2+}]_i$ mobilisation (**Figure 6E**, $p < 0.001$) were significantly reduced compared to those of the hIP. Furthermore, image analysis confirmed that the hIP^{K297Q,R302L,K304Q} did not traffic to the PM, but rather was largely retained in the ER where it co-localised with calnexin (**Figure 6**F). Hence, insertion of the canonical F(X)$_6$LL motif into the sequence of the ER-retained hIP^{K297,304Q} did not rescue the defect and result in its export from the ER to the PM. These data may suggest that the presence of the F(X)$_6$LL motif alone may not be sufficient to drive ER export of this receptor. Alternatively, the hIP^{K297Q,R302L,K304Q} receptor may be terminally misfolded resulting in its accumulation within the ER.

3.6 The Effect of Substitution of Alternative Positively Charged Amino Acids within the Novel Lys^{297}, Arg^{302}, Lys^{304} ER Export Motif on the Expression and Intracellular Signalling of the hIP

Data presented herein suggests that the presence of three positively charged, basic amino acids located at Lys^{297}, Arg^{302} and Lys^{304} within the α-H8 may actually represent a novel ER export motif within the proximal C-tail of the hIP and may be defined as a K^{297}(X)$_4$R^{302}(X)K^{304} or, more generically, as a 'K(X)$_4$R(X)K' ER export motif. It was next sought to further interrogate this ER export motif by investigating whether there was a strict requirement for these exact amino acids in the critical Lys^{297}, Arg^{302} and/or Lys^{304} positions to facilitate export of the hIP from the ER or whether Lys or Arg residues could be substituted for each other in each of those positions. To this end, as with previous approaches, site-directed mutagenesis in conjunction with establishment of the respective clonal HEK 293 cell lines, 4 additional variants of the hIP were generated. These included hIP^{K297R}, hIP^{R302K}, hIP^{K304R} and hIP^{K297,304R} containing all

4 possible variants ('$\mathbf{R}^{297}(X)_4R^{302}(X)K^{304}$', '$K^{297}(X)_4\mathbf{K}^{302}(X)K^{304}$', '$K^{297}(X)_4R^{302}(X)\mathbf{R}^{304}$' and '$\mathbf{R}^{297}(X)_4R^{302}(X)\mathbf{R}^{304}$') of the ER export motif ($K^{297}(X)_4R^{302}(X)K^{304}$) found in the wild type hIP (**Figure 7A**).

Western blot analysis of whole cell protein confirmed that the hIP^{K297R}, hIP^{R302K}, hIP^{K304R} and $hIP^{K297,304R}$ were each expressed as the mature, fully glycosylated species (46 – 66 kDa) and as the immature core glycosylated intermediate species (44 and 42 kDa) in a pattern similar to that of the wild-type hIP (**Figure 7B**). While the hIP^{K297R}, hIP^{R302K}, hIP^{K304R} and $hIP^{K297,304R}$ displayed minor reductions in the levels of [^{3}H]iloprost binding and cicaprost-induced $[Ca^{2+}]_i$ mobilisation relative to those of the hIP, these reductions were not significant (**Figure 7C & 7D**). Furthermore, as displayed for the hIP^{K304R} variant, image analysis confirmed that substituting Lys to Arg residues, and *vice versa,* or converting them to Lys or Arg residues exclusively yielded variant hIPs that displayed normal expression at the PM and did not co-localise with calnexin in the ER (**Figure 7E**). Taken together, these data indicate that it is permissible to substitute one or more basic residues at positions 297, 302 and 304 in the hIP sequence for another basic residue without disrupting the ability of these receptors to be exported from the ER to their functional destination at the PM and, hence, that any of the variant sequences can serve as an ER export motif within the hIP.

Consistent with this, bioinformatic analyses and multi-alignment of the primary IP sequences from various species shows that the $K(X)_4R(X)K$ motif is highly conserved in the proximal C-tail of the human, mouse, rat, cow and chimpanzee (**Figure 8A**). In addition, the equivalent sequence in the equine IP is the variant $K(X)_4R(X)\mathbf{R}$ while that of the canine IP is $K(X)_4\mathbf{K}(X)\mathbf{R}$, indicating the substitution of positively charged, basic amino acids in the core motif is indeed permissible (**Figure 8A**). However, multi-alignment of the equivalent sequences present within members of the broader human prostanoid receptor subfamily (**Figure 8B**), or indeed within the wider GPCR superfamily as a whole (data not shown), established that the novel '$K(X)_4R(X)K$' ER export motif is unique to the IP and is not found in other related prostanoid or unrelated GPCRs.

Taken together, as depicted in **Figure 8C**, consistent with a previous report [43], I-TASSER structural predictions indicate that the hIP is organised into the 7 TM α-helices and contains an α-H8 within its proximal C-tail domain that lies perpendicular to the TM bundle but parallel to the lipid bilayer to which it associates, at least in part, due to palmitoylation at the adjacent Cys^{308}, Cys^{309} and/or Cys^{311} residues. Data herein demonstrate that Lys^{297}, Arg^{302} and Lys^{304} within the α-H8 form the critical residues that define a novel ER export motif within the hIP but that, consistent with sequences naturally occurring in IP orthologues from other species, substitution of Lys or Arg residues within the '$K(X)_4R(X)K$' to generate the variant '$K/R(X)_4$ K/R(X) K/R' is functionally permissible.

4. Discussion

In the present study, a trafficking signal composed of three positively charged, basic amino acids, namely Lys^{297}, Arg^{302} and Lys^{304} or, simply, $K/R(X)_4K/R(X)K/R$, has been identified in the α-H8 domain of the hIP and this is evolutionary conserved in the sequence of the IP from mouse to man.

The life cycle of all GPCRs consists of a number of distinct phases. GPCRs are synthesised and subject to a host of co- and post-translational modification(s) at the ER, including high mannose or core glycosylation, before correctly folded receptors are transported to the Golgi complex. Once at the Golgi, they are further post-translationally modified, including complex glycosylation, before mature receptors are trafficked to their functional destination at the PM [45, 59]. GPCRs become activated upon ligand binding to the extracellular and/or TM domains, leading to rapid phosphorylation, desensitisation and internalisation. Internalised receptors may then be recycled back to the PM or targeted to the lysosomes for degradation [60, 61]. This intracellular trafficking of GPCRs is a tightly regulated and dynamic process, which plays a major part in determining the level of receptor expression at the PM. While the events following ligand binding to GPCRs at the PM have been extensively studied, the processes regulating the anterograde transport of newly synthesised GPCRs from the ER to the PM remain comparatively less well understood. However, recent studies have shed new insights into the key events involved in the trafficking of GPCRs from the ER through the Golgi complex to the PM.

Export of newly synthesised GPCRs from the ER is the first step in intracellular trafficking and it is a dynamic, highly regulated event that has a marked effect on their expression and function at the cell surface. A quality control system is in place in the ER such that only correctly folded and assembled receptors are transported to the Golgi complex [59, 62]. The ER contains molecular chaperones to assist protein folding and to prevent the export of non-native or misfolded proteins. Should misfolded proteins accumulate in the ER, two distinct but interconnected mechanisms may be activated. The unfolded protein response (UPR) acts to increase the folding capacity of the ER by increasing the levels of chaperones and enzymes [63] while the ERAD response recognises terminally misfolded proteins and retrotranslocates them from the ER to the cytosol where they are ubiquitinated and targeted for degradation by the 26S proteasome [64, 65].

GPCRs are now known to be part of multiprotein networks and many accessory proteins interact with them to mediate or modulate their signalling [66]. These GPCR-interacting proteins (GIPs), such as receptor activity modifying proteins (RAMPs) and the Homer proteins, may also directly interact with GPCRs to stabilise their conformation and therefore enhance maturation [44, 67, 68]. Furthermore, it has now become accepted that many GPCRs exist as dimers and/or oligomers [69, 70]. Dimerisation of some GPCRs has been demonstrated to occur in the ER and this may be required for their ER export, as demonstrated for the metabotropic γ-aminobutyric acid (GABA) receptor and the β_2-AR [71, 72]. Trafficking of GPCRs is also regulated by a large variety of Rab GTPases which act as key molecular switches to integrate intracellular signalling and are involved in all facets of vesicular protein transport [73, 74].

In addition to such events and interacting proteins, a number of structural motifs have been identified in the primary sequence of many GPCRs which play a major role in their export from the ER [44, 45]. Once correctly folded, GPCRs enter ER exit sites where they are exported to the Golgi complex. Protein transport from the ER is mediated exclusively by coat protein (COP)II vesicles and many GPCRs possess these specific ER export motifs which may bind to components of the COPII vesicles [44]. To date, most of the ER export motifs identified have been located in the proximal C-tail domain of GPCRs and contain hydrophobic amino acids. The $E(X)_3LL$ motif (where E is Glu, X is any amino acid and L is Leu) is essential for cell surface targeting of the V2 vasopressin receptor [75]. The $F(X)_3F(X)_3F$ motif (where F is Phe and X is any amino acid) is required for cell surface expression of the dopamine 1 receptor (D1R) [76]. Likewise, the $FN(X)_2LL(X)_3L$ motif (where F is Phe, N is Asn, X is any amino acid and L is Leu) is required for ER export of the human vasopressinV1b/V3 receptor [77]. Furthermore, as outlined earlier, the $F(X)_6LL$ motif (where F is Phe, X is any amino acid and L is Leu or Ile) is required, at least in part, for export of the α_{2B}-AR, the α_{1B}-AR, the β_2-AR and the AT1R from the ER [46, 47]. In fact, this $F(X)_6LL$ motif is highly conserved in the C-tail domain of many, but not all, GPCRs and is postulated to provide a common mechanism directing ER to cell surface trafficking of GPCRs [47]. It should also be noted that while the majority of the ER export motifs identified to date are located in the membrane-proximal C-tail domain, additional studies have identified putative motifs in different regions of GPCRs which may be responsible, at least in part, for ER export. For example, a single Met residue in the N-terminus and a single conserved Leu residue in IC_1 loop also appear to be required for ER export of the α_{2B}-AR [78, 79].

While such structural motifs are responsible for the export of GPCRs from the ER, other ER retention signals/motifs have been also identified which actually prevent even correctly folded proteins being transported from the ER. For example, the RXR motif (where R is Arg and X is any amino acid), originally identified in the ATP-sensitive K^+ channel, prevents the export of proteins from the ER [80]. Alternatively, other motifs such as the KDEL (where K is Lys, D is Asp, E is Glu and L is Leu) and the KKXX (where K is Lys and X is any amino acid) motifs are believed to function as retrieval signals by recycling proteins from the Golgi complex back to the ER [81]. More recently, an evolutionary conserved hydrophobic sequence in the extracellular N-terminus of the α_{2C}-AR was shown to regulate its cellular processing and PM expression. The wild-type α_{2C}-AR contains the sequence ALAAALAAAAA (where A is Ala and L is Leu) and is normally retained in the ER in Rat1 fibroblast and HEK293 cells. Removal of this sequence significantly improves PM expression of the receptor [82].

In the current study, analysis of the C-tail domain of the hIP did not reveal a sequence matching any of the currently known ER export or ER retention motifs typically associated with GPCRs. Therefore, it was sought to identify the sequences required for transport of the hIP from the ER to the PM. To this end, through mutational analysis, Lys^{297} and Lys^{304} were found to be critical for maturation of the hIP while *Ala-scanning* mutagenesis also identified Arg^{302} as the only other residue important for normal trafficking of the hIP. Therefore, these data suggested that Lys^{297}, Arg^{302} and Lys^{304} constituted a putative ER export motif solely composed of positively charged, basic amino acids, defined by $K(X)_4R(X)K$, which were absolutely required for the export of the wild-type hIP from the ER to its functional destination at the PM.

Subsequently, it was established that it was indeed permissible to substitute one or more of these Lys or Arg residues for another positively charged residue without affecting the ability of the resulting receptors to be exported from the ER to the PM in a manner similar to the wild-type hIP. Moreover, alignment of the primary sequences of the IP from a number of mammalian species verified that the variant $K/R(X)_4K/R(X)K/R$ motif is evolutionarily conserved and, hence, substitution of one positively charged residue of the sequence for another is functionally permissible.

These Lys^{297}, Arg^{302} and Lys^{304} basic residues are also of significant interest because they lie within the putative eighth α-helical domain (α-H8) of the hIP. The first evidence for the existence of this α-H8 arose from x-ray crystallography studies of the rhodopsin receptor [4]. This domain lies parallel to the PM and perpendicular to the TM helices, and it was well positioned to directly interact with the PM, such as through acylation/palmitoylation of nearby Cys residue(s). In contrast, the α-H8 may adopt a loop-like or disordered structure in an aqueous environment or in the conformationally active receptor [7, 83, 84]. Further experimental and computational studies predicted that the α-H8 is likely to be a general feature of GPCRs which, significantly, was also shown to be important for many of their functions, such as expression and intracellular trafficking, G-protein coupling and activation, dimerisation, internalisation and signalling [6-8, 10].

Rab11a mediates the recycling of certain GPCRs, including the hIP, from the endosomal recycling compartment to the PM via the so-called "long" recycling pathway [42]. In the case of the hIP, a direct interaction between its α-H8 domain and Rab11a was recently established [34]. This represented the first demonstration of a direct interaction between Rab11a and the α-H8 domain of any GPCR and the Rab11a-binding domain (RBD) of the hIP was localised to a sequence of 14 residues spanning the region from Val^{299} – Leu^{312} including a major part of α-H8 (Val^{299} – Val^{307}) adjacent to the palmitoylated residues at Cys^{308} – Cys^{311} [34]. In that study, the entire RBD domain of the hIP was subject to *Ala-scanning* mutagenesis and it was established that the hydrophobic residues Phe^{300}, Leu^{303}, Leu^{305} and Val^{307}, mainly orientated on one face of the α-H8 domain, provide the interface to which Rab11a actually binds [34]. In addition, evidence for a role for the positively charged Arg^{302} and Lys^{304} residues in influencing the interaction between the hIP and Rab11a was also provided, but could not be verified due to the failure of the hIP^{R302A} and hIP^{K304A} variants to be expressed at the PM. I-TASSER simulations [56, 57] predict that in the optimal hIP structure, the positively charged Lys^{297} and Lys^{304} lie on the same face of the α-H8 domain opposite to that of Arg^{302} (**Figure 8C**; plane and cross-sectional views). Importantly, however, the structure and indeed orientation of those residues in the newly synthesised hIP temporarily resident in the ER, *en route* to its ultimate functional destination at the PM, is unknown. Accordingly, the $K(X)_4R(X)K$ motif is likely to be important in the early stages of the life cycle of the hIP by mediating its transport from the ER to the Golgi complex, perhaps by facilitating the interaction of the correctly folded receptor in the ER with components of the COPII vesicles. It is possible that some or all of these residues in α-H8 that are involved in ER to Golgi transport may also be required to facilitate further interactions of the hIP, for example, with other Rab(s) such as at different stages of the life cycle of the hIP. Rab proteins are localised to the cytosolic face of

intracellular membranes where they regulate distinct steps in membrane trafficking [74, 85]. Rab1 is localised to the ER and the Golgi and is involved in anterograde transport of certain GPCRs from the ER to the Golgi and within the Golgi itself [86-88]. Rab8 regulates post-Golgi trafficking of certain GPCRs, such as the α_{2B}-AR and the β_2-AR, and this was shown to occur through a direct interaction of the latter receptors with Rab8 [89]. As mentioned previously, Arg^{302} and Lys^{304} of the hIP appear to be required, at least in part, for its interaction with Rab11a, which is involved in recycling of internalised hIP to the PM [34]. Therefore, disruption of the $K(X)_4R(X)K$ ER export motif may also disrupt association of the hIP with a member(s) of the Rab family of proteins, which are highly involved in intracellular trafficking of GPCRs. Such possible interactions with specific members of the Rab family of 70 proteins or other unidentified proteins are, of course, entirely speculative at this point and greater clarification would require extensive additional experimentation to identify such protein(s).

The importance of a cluster of positively charged, basic amino acids in the C-tail domain of GPCRs for their trafficking from the ER through to the Golgi complex and onwards to the cell surface has previously been shown for certain other receptors. For example, a membrane-proximal basic domain, in conjunction with a neighbouring cluster of Cys residues that are targets for palmitoylation, was absolutely required for efficient transport and expression of the CCR5 chemokine receptor at the cell surface [90]. Mutation of Arg^{319}, Lys^{320} or Arg^{321} in α-H8 of the melanin-concentrating hormone 1 receptor (MCH1R) led to a decrease in cell surface expression and, furthermore, a significant decrease in calcium influx was evident with the $Arg^{319}$and Lys^{320} single or double mutants but not with the Arg^{321} mutant [91]. Additionally, the human follicle stimulating hormone receptor (hFSHR) possesses two basic BXXBB motifs (where B represents a basic amino acid residue and X a non-basic residue) in the juxtamembrane region of its IC_3 loop and the C-tail, respectively. The basic motif in IC_3 loop was required for coupling of the activated receptor to $G\alpha_s$, whereas the motif in the C-tail was required for PM expression [92].

While the studies presented herein are exclusively based on a heterologous expression system, these data do provide the first evidence for the presence of a structural motif composed of three basic amino acids with the sequence $K/R(X)_4K/R(X)K/R$ in the α-H8 of the hIP which is absolutely required for its export from the ER and expression at the PM. To highlight its importance, it appears that this basic motif is evolutionarily conserved in the IP from a number of other mammalian species. However, it is noteworthy that this transmembrane-proximal α-H8 of the hIP is potentially involved in a number of complex interactions with intracellular proteins. Trafficking and processing of the hIP is a complicated process relying not only on the presence of this ER export motif in α-H8 but also on the coordination of a host of other events such that functional receptors may be expressed at the PM. Defective protein transport has been linked to the pathogenesis of a variety of human diseases, including cystic fibrosis and Alzheimer's disease [93]. Therefore, it would be of interest to further define the molecular mechanism by which the $K/R(X)_4K/R(X)K/R$ motif regulates ER export of the hIP and to identify the protein(s) selectively interacting with this motif. Moreover, numerous nonsynonymous mutations have been identified within the coding sequence of the hIP that are linked with increased risk of deep vein thrombosis and the dysfunctional R212C mutation is associated with intimal hyperplasia [23]. Hence, further knowledge of the factors regulating the

maturation and functional expression of the hIP is essential and may provide a rationale for the identification of therapeutic or surrogate approaches to rescue its expression where normal physiologic function is impaired.

Acknowledgements

We are grateful to Dr Natalia Jura, Stony Brook University Cold Spring Harbor Laboratory, NY, U.S.A. for the gift of the plasmid encoding YFP-β-Gal and to Bayer Schering AG (Berlin, Germany) for the gift of cicaprost. This work was supported by grants to BTK from Science Foundation of Ireland (Grant No. SFI: 05/IN.1/B19) and Health Research Board (Grant No. RP/2008/33).

REFERENCES

[1] M.C. Lagerstrom, H.B. Schioth, Structural diversity of G protein-coupled receptors and significance for drug discovery, Nat Rev Drug Discov 7 (2008) 339-357.

[2] M.N. Davies, A. Secker, A.A. Freitas, M. Mendao, J. Timmis, D.R. Flower, On the hierarchical classification of G protein-coupled receptors, Bioinformatics (Oxford, England) 23 (2007) 3113-3118.

[3] K.L. Pierce, R.T. Premont, R.J. Lefkowitz, Seven-transmembrane receptors, Nature reviews 3 (2002) 639-650.

[4] K. Palczewski, T. Kumasaka, T. Hori, C.A. Behnke, H. Motoshima, B.A. Fox, I. Le Trong, D.C. Teller, T. Okada, R.E. Stenkamp, M. Yamamoto, M. Miyano, Crystal structure of rhodopsin: A G protein-coupled receptor, Science (New York, N.Y 289 (2000) 739-745.

[5] D.M. Rosenbaum, S.G. Rasmussen, B.K. Kobilka, The structure and function of G-protein-coupled receptors, Nature 459 (2009) 356-363.

[6] N.M. Delos Santos, L.A. Gardner, S.W. White, S.W. Bahouth, Characterization of the residues in helix 8 of the human beta1-adrenergic receptor that are involved in coupling the receptor to G proteins, The Journal of biological chemistry 281 (2006) 12896-12907.

[7] M. Katragadda, M.W. Maciejewski, P.L. Yeagle, Structural studies of the putative helix 8 in the human beta(2) adrenergic receptor: an NMR study, Biochimica et biophysica acta 1663 (2004) 74-81.

[8] V.P. Jaakola, M.T. Griffith, M.A. Hanson, V. Cherezov, E.Y. Chien, J.R. Lane, A.P. Ijzerman, R.C. Stevens, The 2.6 angstrom crystal structure of a human A2A adenosine receptor bound to an antagonist, Science (New York, N.Y 322 (2008) 1211-1217.

[9] G. Milligan, G protein-coupled receptor dimerisation: molecular basis and relevance to function, Biochimica et biophysica acta 1768 (2007) 825-835.

[10] J. Huynh, W.G. Thomas, M.I. Aguilar, L.K. Pattenden, Role of helix 8 in G protein-coupled receptors based on structure-function studies on the type 1 angiotensin receptor, Molecular and cellular endocrinology 302 (2009) 118-127.

[11] R.J. Gryglewski, Prostacyclin among prostanoids, Pharmacol Rep 60 (2008) 3-11.

[12] K.R. Bley, J.C. Hunter, R.M. Eglen, J.A. Smith, The role of IP prostanoid receptors in inflammatory pain, Trends in pharmacological sciences 19 (1998) 141-147.

[13] T. Murata, F. Ushikubi, T. Matsuoka, M. Hirata, A. Yamasaki, Y. Sugimoto, A. Ichikawa, Y. Aze, T. Tanaka, N. Yoshida, A. Ueno, S. Oh-ishi, S. Narumiya, Altered pain perception and inflammatory response in mice lacking prostacyclin receptor, Nature 388 (1997) 678-682.

[14] Y. Cheng, S.C. Austin, B. Rocca, B.H. Koller, T.M. Coffman, T. Grosser, J.A. Lawson, G.A. FitzGerald, Role of prostacyclin in the cardiovascular response to thromboxane A2, Science (New York, N.Y 296 (2002) 539-541.

[15] S. Narumiya, Y. Sugimoto, F. Ushikubi, Prostanoid receptors: structures, properties, and functions, Physiological reviews 79 (1999) 1193-1226.

[16] L.G. Ribeiro, T.A. Brandon, D.G. Hopkins, L.A. Reduto, A.A. Taylor, R.R. Miller, Prostacyclin in experimental myocardial ischemia: effects on hemodynamics, regional myocardial blood flow, infarct size and mortality, Am J Cardiol 47 (1981) 835-840.

[17] J. Kawabe, K. Yuhki, M. Okada, T. Kanno, A. Yamauchi, N. Tashiro, T. Sasaki, S. Okumura, N. Nakagawa, Y. Aburakawa, N. Takehara, T. Fujino, N. Hasebe, S. Narumiya, F. Ushikubi, Prostaglandin I2 promotes recruitment of endothelial progenitor cells and limits vascular remodeling, Arterioscler Thromb Vasc Biol 30 (2010) 464-470.

[18] S. Krug, A. Sablotzki, S. Hammerschmidt, H. Wirtz, H.J. Seyfarth, Inhaled iloprost for the control of pulmonary hypertension, Vascular health and risk management 5 (2009) 465-474.

[19] Y. Sugimoto, S. Narumiya, A. Ichikawa, Distribution and function of prostanoid receptors: studies from knockout mice, Progress in lipid research 39 (2000) 289-314.

[20] K.M. Egan, J.A. Lawson, S. Fries, B. Koller, D.J. Rader, E.M. Smyth, G.A. Fitzgerald, COX-2-derived prostacyclin confers atheroprotection on female mice, Science (New York, N.Y 306 (2004) 1954-1957.

[21] T. Kobayashi, Y. Tahara, M. Matsumoto, M. Iguchi, H. Sano, T. Murayama, H. Arai, H. Oida, T. Yurugi-Kobayashi, J.K. Yamashita, H. Katagiri, M. Majima, M. Yokode, T. Kita, S. Narumiya,

Roles of thromboxane A(2) and prostacyclin in the development of atherosclerosis in apoE-deficient mice, The Journal of clinical investigation 114 (2004) 784-794.

[22] E. Arehart, J. Stitham, F.W. Asselbergs, K. Douville, T. MacKenzie, K.M. Fetalvero, S. Gleim, Z. Kasza, Y. Rao, L. Martel, S. Segel, J. Robb, A. Kaplan, M. Simons, R.J. Powell, J.H. Moore, E.B. Rimm, K.A. Martin, J. Hwa, Acceleration of cardiovascular disease by a dysfunctional prostacyclin receptor mutation: potential implications for cyclooxygenase-2 inhibition, Circulation research 102 (2008) 986-993.

[23] P. Patrignani, C. Di Febbo, S. Tacconelli, K. Douville, M.D. Guglielmi, R.J. Horvath, M. Ding, K. Sierra, J. Stitham, S. Gleim, G. Baccante, V. Moretta, L. Di Francesco, M.L. Capone, E. Porreca, J. Hwa, Differential association between human prostacyclin receptor polymorphisms and the development of venous thrombosis and intimal hyperplasia: a clinical biomarker study, Pharmacogenetics and genomics 18 (2008) 611-620.

[24] R.A. Coleman, S.P. Grix, S.A. Head, J.B. Louttit, A. Mallett, R.L. Sheldrick, A novel inhibitory prostanoid receptor in piglet saphenous vein, Prostaglandins 47 (1994) 151-168.

[25] R.L. Hebert, T. O'Connor, C. Neville, K.D. Burns, O. Laneuville, L.N. Peterson, Prostanoid signaling, localization, and expression of IP receptors in rat thick ascending limb cells, The American journal of physiology 275 (1998) F904-914.

[26] O.A. Lawler, S.M. Miggin, B.T. Kinsella, Protein kinase A-mediated phosphorylation of serine 357 of the mouse prostacyclin receptor regulates its coupling to G(s)-, to G(i)-, and to G(q)-coupled effector signaling, The Journal of biological chemistry 276 (2001) 33596-33607.

[27] S.M. Miggin, B.T. Kinsella, Investigation of the mechanisms of G protein: effector coupling by the human and mouse prostacyclin receptors. Identification of critical species-dependent differences, The Journal of biological chemistry 277 (2002) 27053-27064.

[28] R. Schubert, V.N. Serebryakov, H. Mewes, H.H. Hopp, Iloprost dilates rat small arteries: role of K(ATP)- and K(Ca)-channel activation by cAMP-dependent protein kinase, The American journal of physiology 272 (1997) H1147-1156.

[29] G. Siegel, A. Carl, A. Adler, G. Stock, Effect of the prostacyclin analogue iloprost on K+ permeability in the smooth muscle cells of the canine carotid artery, Eicosanoids 2 (1989) 213-222.

[30] E.M. Smyth, P.V. Nestor, G.A. FitzGerald, Agonist-dependent phosphorylation of an epitope-tagged human prostacyclin receptor, The Journal of biological chemistry 271 (1996) 33698-33704.

[31] Z. Zhang, S.C. Austin, E.M. Smyth, Glycosylation of the human prostacyclin receptor: role in ligand binding and signal transduction, Molecular pharmacology 60 (2001) 480-487.

[32] S.M. Miggin, O.A. Lawler, B.T. Kinsella, Investigation of a functional requirement for isoprenylation by the human prostacyclin receptor, European journal of biochemistry / FEBS 269 (2002) 1714-1725.

[33] S.M. Miggin, O.A. Lawler, B.T. Kinsella, Palmitoylation of the human prostacyclin receptor. Functional implications of palmitoylation and isoprenylation, The Journal of biological chemistry 278 (2003) 6947-6958.

[34] H.M. Reid, E.P. Mulvaney, E.C. Turner, B.T. Kinsella, Interaction of the human prostacyclin receptor with Rab11: characterization of a novel Rab11 binding domain within alpha-helix 8 that is regulated by palmitoylation, The Journal of biological chemistry 285 18709-18726.

[35] P.D. Donnellan, B.T. Kinsella, Immature and mature species of the human Prostacyclin Receptor are ubiquitinated and targeted to the 26S proteasomal or lysosomal degradation pathways, respectively, Journal of molecular signaling 4 (2009) 7.

[36] J.L. Seachrist, S.S. Ferguson, Regulation of G protein-coupled receptor endocytosis and trafficking by Rab GTPases, Life Sci 74 (2003) 225-235.

[37] S. Christoforidis, H.M. McBride, R.D. Burgoyne, M. Zerial, The Rab5 effector EEA1 is a core component of endosome docking, Nature 397 (1999) 621-625.

[38] S. de Renzis, B. Sonnichsen, M. Zerial, Divalent Rab effectors regulate the sub-compartmental organization and sorting of early endosomes, Nature cell biology 4 (2002) 124-133.

[39] K. Mohrmann, P. van der Sluijs, Regulation of membrane transport through the endocytic pathway by rabGTPases, Molecular membrane biology 16 (1999) 81-87.

[40] B. Sonnichsen, S. De Renzis, E. Nielsen, J. Rietdorf, M. Zerial, Distinct membrane domains on endosomes in the recycling pathway visualized by multicolor imaging of Rab4, Rab5, and Rab11, J Cell Biol 149 (2000) 901-914.

[41] M.B. O'Keeffe, H.M. Reid, B.T. Kinsella, Agonist-dependent internalization and trafficking of the human prostacyclin receptor: a direct role for Rab5a GTPase, Biochimica et biophysica acta 1783 (2008) 1914-1928.
[42] K. Wikstrom, H.M. Reid, M. Hill, K.A. English, M.B. O'Keeffe, C.C. Kimbembe, B.T. Kinsella, Recycling of the human prostacyclin receptor is regulated through a direct interaction with Rab11a GTPase, Cellular signalling 20 (2008) 2332-2346.
[43] H.M. Reid, E.P. Mulvaney, E.C. Turner, B.T. Kinsella, Interaction of the human prostacyclin receptor with Rab11: characterization of a novel Rab11 binding domain within alpha-helix 8 that is regulated by palmitoylation, The Journal of biological chemistry 285 (2010) 18709-18726.
[44] C. Dong, C.M. Filipeanu, M.T. Duvernay, G. Wu, Regulation of G protein-coupled receptor export trafficking, Biochimica et biophysica acta 1768 (2007) 853-870.
[45] C.M. Tan, A.E. Brady, H.H. Nickols, Q. Wang, L.E. Limbird, Membrane trafficking of G protein-coupled receptors, Annual review of pharmacology and toxicology 44 (2004) 559-609.
[46] M.T. Duvernay, C. Dong, X. Zhang, F. Zhou, C.D. Nichols, G. Wu, Anterograde trafficking of G protein-coupled receptors: function of the C-terminal F(X)6LL motif in export from the endoplasmic reticulum, Molecular pharmacology 75 (2009) 751-761.
[47] M.T. Duvernay, F. Zhou, G. Wu, A conserved motif for the transport of G protein-coupled receptors from the endoplasmic reticulum to the cell surface, The Journal of biological chemistry 279 (2004) 30741-30750.
[48] N. Jura, E. Scotto-Lavino, A. Sobczyk, D. Bar-Sagi, Differential modification of Ras proteins by ubiquitination, Molecular cell 21 (2006) 679-687.
[49] O.A. Lawler, S.M. Miggin, B.T. Kinsella, The effects of the statins lovastatin and cerivastatin on signalling by the prostanoid IP-receptor, Br J Pharmacol 132 (2001) 1639-1649.
[50] C.M. Gorman, D. Gies, G. McCray, Transient production of proteins using an adenovirus transformed cell line., DNA Protein Eng. Tech. 2 (1990) 3-10.
[51] B.T. Kinsella, D.J. O'Mahony, G.A. Fitzgerald, The human thromboxane A2 receptor alpha isoform (TP alpha) functionally couples to the G proteins Gq and G11 in vivo and is activated by the isoprostane 8-epi prostaglandin F2 alpha, J Pharmacol Exp Ther 281 (1997) 957-964.
[52] J.S. Hayes, O.A. Lawler, M.T. Walsh, B.T. Kinsella, The prostacyclin receptor is isoprenylated. Isoprenylation is required for efficient receptor-effector coupling, The Journal of biological chemistry 274 (1999) 23707-23718.
[53] M.M. Bradford, A rapid and sensitive method for the quantitation of microgram quantities of protein utilizing the principle of protein-dye binding, Anal Biochem 72 (1976) 248-254.
[54] G. Grynkiewicz, M. Poenie, R.Y. Tsien, A new generation of Ca2+ indicators with greatly improved fluorescence properties, The Journal of biological chemistry 260 (1985) 3440-3450.
[55] K.R. Gee, K.A. Brown, W.N. Chen, J. Bishop-Stewart, D. Gray, I. Johnson, Chemical and physiological characterization of fluo-4 Ca(2+)-indicator dyes, Cell Calcium 27 (2000) 97-106.
[56] Y. Zhang, Template-based modeling and free modeling by I-TASSER in CASP7, Proteins 69 Suppl 8 (2007) 108-117.
[57] Y. Zhang, I-TASSER server for protein 3D structure prediction, BMC bioinformatics 9 (2008) 40.
[58] C. Cole, J.D. Barber, G.J. Barton, The Jpred 3 secondary structure prediction server, Nucleic acids research 36 (2008) W197-201.
[59] L. Ellgaard, A. Helenius, Quality control in the endoplasmic reticulum, Nature reviews 4 (2003) 181-191.
[60] M.T. Drake, S.K. Shenoy, R.J. Lefkowitz, Trafficking of G protein-coupled receptors, Circulation research 99 (2006) 570-582.
[61] A. Marchese, C. Chen, Y.M. Kim, J.L. Benovic, The ins and outs of G protein-coupled receptor trafficking, Trends in biochemical sciences 28 (2003) 369-376.
[62] B. Bukau, J. Weissman, A. Horwich, Molecular chaperones and protein quality control, Cell 125 (2006) 443-451.
[63] M. Schroder, R.J. Kaufman, The mammalian unfolded protein response, Annual review of biochemistry 74 (2005) 739-789.
[64] B. Tsai, Y. Ye, T.A. Rapoport, Retro-translocation of proteins from the endoplasmic reticulum into the cytosol, Nature reviews 3 (2002) 246-255.
[65] B. Meusser, C. Hirsch, E. Jarosch, T. Sommer, ERAD: the long road to destruction, Nature cell biology 7 (2005) 766-772.

[66] S.L. Ritter, R.A. Hall, Fine-tuning of GPCR activity by receptor-interacting proteins, Nature reviews 10 (2009) 819-830.
[67] F. Ango, D. Robbe, J.C. Tu, B. Xiao, P.F. Worley, J.P. Pin, J. Bockaert, L. Fagni, Homer-dependent cell surface expression of metabotropic glutamate receptor type 5 in neurons, Molecular and cellular neurosciences 20 (2002) 323-329.
[68] L.M. McLatchie, N.J. Fraser, M.J. Main, A. Wise, J. Brown, N. Thompson, R. Solari, M.G. Lee, S.M. Foord, RAMPs regulate the transport and ligand specificity of the calcitonin-receptor-like receptor, Nature 393 (1998) 333-339.
[69] M. Bai, Dimerization of G-protein-coupled receptors: roles in signal transduction, Cellular signalling 16 (2004) 175-186.
[70] M. Bouvier, Oligomerization of G-protein-coupled transmitter receptors, Nat Rev Neurosci 2 (2001) 274-286.
[71] K.A. Jones, B. Borowsky, J.A. Tamm, D.A. Craig, M.M. Durkin, M. Dai, W.J. Yao, M. Johnson, C. Gunwaldsen, L.Y. Huang, C. Tang, Q. Shen, J.A. Salon, K. Morse, T. Laz, K.E. Smith, D. Nagarathnam, S.A. Noble, T.A. Branchek, C. Gerald, GABA(B) receptors function as a heteromeric assembly of the subunits GABA(B)R1 and GABA(B)R2, Nature 396 (1998) 674-679.
[72] A. Salahpour, S. Angers, J.F. Mercier, M. Lagace, S. Marullo, M. Bouvier, Homodimerization of the beta2-adrenergic receptor as a prerequisite for cell surface targeting, The Journal of biological chemistry 279 (2004) 33390-33397.
[73] S.R. Pfeffer, Structural clues to Rab GTPase functional diversity, The Journal of biological chemistry 280 (2005) 15485-15488.
[74] M. Zerial, H. McBride, Rab proteins as membrane organizers, Nature reviews 2 (2001) 107-117.
[75] R. Schulein, R. Hermosilla, A. Oksche, M. Dehe, B. Wiesner, G. Krause, W. Rosenthal, A dileucine sequence and an upstream glutamate residue in the intracellular carboxyl terminus of the vasopressin V2 receptor are essential for cell surface transport in COS.M6 cells, Molecular pharmacology 54 (1998) 525-535.
[76] J.C. Bermak, M. Li, C. Bullock, Q.Y. Zhou, Regulation of transport of the dopamine D1 receptor by a new membrane-associated ER protein, Nature cell biology 3 (2001) 492-498.
[77] J. Robert, E. Clauser, P.X. Petit, M.A. Ventura, A novel C-terminal motif is necessary for the export of the vasopressin V1b/V3 receptor to the plasma membrane, The Journal of biological chemistry 280 (2005) 2300-2308.
[78] C. Dong, G. Wu, Regulation of anterograde transport of alpha2-adrenergic receptors by the N termini at multiple intracellular compartments, The Journal of biological chemistry 281 (2006) 38543-38554.
[79] M.T. Duvernay, C. Dong, X. Zhang, M. Robitaille, T.E. Hebert, G. Wu, A Single Conserved Leucine Residue on the First Intracellular Loop Regulates ER Export of G Protein-Coupled Receptors, Traffic (Copenhagen, Denmark) (2009).
[80] N. Zerangue, B. Schwappach, Y.N. Jan, L.Y. Jan, A new ER trafficking signal regulates the subunit stoichiometry of plasma membrane K(ATP) channels, Neuron 22 (1999) 537-548.
[81] M. Stornaiuolo, L.V. Lotti, N. Borgese, M.R. Torrisi, G. Mottola, G. Martire, S. Bonatti, KDEL and KKXX retrieval signals appended to the same reporter protein determine different trafficking between endoplasmic reticulum, intermediate compartment, and Golgi complex, Molecular biology of the cell 14 (2003) 889-902.
[82] T. Angelotti, D. Daunt, O.G. Shcherbakova, B. Kobilka, C.M. Hurt, Regulation of G-protein coupled receptor traffic by an evolutionary conserved hydrophobic signal, Traffic (Copenhagen, Denmark) 11 560-578.
[83] S. Topiol, M. Sabio, X-ray structure breakthroughs in the GPCR transmembrane region, Biochemical pharmacology 78 (2009) 11-20.
[84] P.L. Yeagle, A.D. Albert, G-protein coupled receptor structure, Biochimica et biophysica acta 1768 (2007) 808-824.
[85] S.L. Schwartz, C. Cao, O. Pylypenko, A. Rak, A. Wandinger-Ness, Rab GTPases at a glance, Journal of cell science 120 (2007) 3905-3910.
[86] G. Wu, G. Zhao, Y. He, Distinct pathways for the trafficking of angiotensin II and adrenergic receptors from the endoplasmic reticulum to the cell surface: Rab1-independent transport of a G protein-coupled receptor, The Journal of biological chemistry 278 (2003) 47062-47069.

[87] C.M. Filipeanu, F. Zhou, W.C. Claycomb, G. Wu, Regulation of the cell surface expression and function of angiotensin II type 1 receptor by Rab1-mediated endoplasmic reticulum-to-Golgi transport in cardiac myocytes, The Journal of biological chemistry 279 (2004) 41077-41084.

[88] C.M. Filipeanu, F. Zhou, E.K. Fugetta, G. Wu, Differential regulation of the cell-surface targeting and function of beta- and alpha1-adrenergic receptors by Rab1 GTPase in cardiac myocytes, Molecular pharmacology 69 (2006) 1571-1578.

[89] C. Dong, L. Yang, X. Zhang, H. Gu, M.L. Lam, W.C. Claycomb, H. Xia, G. Wu, Rab8 interacts with distinct motifs in alpha2B- and beta2-adrenergic receptors and differentially modulates their transport, The Journal of biological chemistry 285 20369-20380.

[90] S. Venkatesan, A. Petrovic, M. Locati, Y.O. Kim, D. Weissman, P.M. Murphy, A membrane-proximal basic domain and cysteine cluster in the C-terminal tail of CCR5 constitute a bipartite motif critical for cell surface expression, The Journal of biological chemistry 276 (2001) 40133-40145.

[91] M. Tetsuka, Y. Saito, K. Imai, H. Doi, K. Maruyama, The basic residues in the membrane-proximal C-terminal tail of the rat melanin-concentrating hormone receptor 1 are required for receptor function, Endocrinology 145 (2004) 3712-3723.

[92] C. Timossi, C. Ortiz-Elizondo, D.B. Pineda, J.A. Dias, P.M. Conn, A. Ulloa-Aguirre, Functional significance of the BBXXB motif reversed present in the cytoplasmic domains of the human follicle-stimulating hormone receptor, Molecular and cellular endocrinology 223 (2004) 17-26.

[93] M. Aridor, L.A. Hannan, Traffic jam: a compendium of human diseases that affect intracellular transport processes, Traffic (Copenhagen, Denmark) 1 (2000) 836-851.

[94] D.G. Higgins, J.D. Thompson, T.J. Gibson, Using CLUSTAL for multiple sequence alignments, Methods in enzymology 266 (1996) 383-402.

Table I Templates and oligonucleotide primers used for site-directed mutagenesis of the hIP

Plasmid	Template	Oligonucleotide Primer
pHM6:hIP^{K218Q}	pHM6:hIP^{WT}	5'- TACCCGCCAGGAG***CAG***CGCCACCAGGGC -3'
pHM6:hIP^{K297Q}	pHM6:hIP^{WT}	5'- CATCCTTTTCCGC***CAG***GCTGTCTTCCAGC -3'
pHM6:hIP^{K304Q}	pHM6:hIP^{WT}	5'- TTCCAGCGACTC***CAG***CTCTGGGTCTGC -3'
pHM6:hIP^{K342Q}	pHM6:hIP^{WT}	5'- GCTCCTGTGGGA***CAG***GAGGGGAGCTGC -3'
pHM6:hIP^{K376Q}	pHM6:hIP^{WT}	5'- GTGGGAACGTCGTCC**C**AAGCAGAAGCCAG -3'
pHM6:hIP^{K297,304Q}	pHM6:hIP^{WT}	5'- GTCTTCATCCTTTTCCGC***CAG***GCTGTCTTCCAG CGACTC***CAG***CTCTGGGTCTGCTG -3'
pHM6:hIP^{K342,376Q}	pHM6:hIP^{K376Q}	5'- GCTCCTGTGGGA***CAG***GAGGGGAGCTGC -3'
pHM6:hIP^{K297,304,342Q}	pHM6:hIP^{K342Q}	5'- GTCTTCATCCTTTTCCGC***CAG***GCTGTCTTCCAGCG ACTC***CAG***CTCTGGGTCTGCTG -3'
pHM6:hIP^{K297,304,376Q}	pHM6:hIP^{K376Q}	5'- GTCTTCATCCTTTTCCGC***CAG***GCTGTCTTCCAGCG ACTC***CAG***CTCTGGGTCTGCTG -3'
pHM6:hIP^{K297,304,342,376Q}	pHM6:hIP^{K342,376Q}	5'- GTCTTCATCCTTTTCCGC***CAG***GCTGTCTTCCAGCG ACTC***CAG***CTCTGGGTCTGCTG -3'
pHM6:hIP^{K218,297,304,342,376Q}	pHM6:hIP^{K297,304,342,376Q}	5'-TACCCGCCAGGAG***CAG***CGCCACCAGGGC- 3'
pHM6:hIP^{K297A}	pHM6:hIP^{WT}	5'- CTTCATCCTTTTCCGC***GCG***GCTGTCTTCCAGCGAC-3'
pHM6:hIP^{K304A}	pHM6:hIP^{WT}	5'- GTCTTCCAGCGACTC***GCG***CTCTGGGTCTGCTGC -3'
pHM6:hIP^{K376A}	pHM6:hIP^{WT}	5'- GTGGGAACGTCGTCC***GCA***GCAGAAGCCAG -3'
pHM6:hIP^{K297,304A}	pHM6:hIP^{K304A}	5'- CTTCATCCTTTTCCGC***GCG***GCTGTCTTCCAGCGAC - 3'
pHM6:hIP^{A298G}	pHM6:hIP^{WT}	5'- CCTTTTCCGCAAG***GGC***GTCTTCCAGCGAC -3'
pHM6:hIP^{V299A}	pHM6:hIP^{WT}	5'- CCTTTTCCGCAAGGCT***GCC***TTCCAGCGACTCAAGC -3'
pHM6:hIP^{F300A}	pHM6:hIP^{WT}	5'- CCGCAAGGCTGTC***GCC***CAGCGACTCAAGC -3'
pHM6:hIP^{Q301A}	pHM6:hIP^{WT}	5'- CGCAAGGCTGTCTTC***GCG***CGACTCAAGCTC -3'
pHM6:hIP^{R302A}	pHM6:hIP^{WT}	5'- AAGGCTGTCTTCCAG***GCA***CTCAAGCTCTGGGTC -3'
pHM6:hIP^{L303A}	pHM6:hIP^{WT}	5'- GCTGTCTTCCAGCGA***GCC***AAGCTCTGGGTC -3'
pHM6:hIP^{K297Q,R302L,K304Q}	pHM6:hIP^{K297,304Q}	5'- GCTGTCTTCCAG***CTC***CTCCAGCTCTGGGTC -3'
pHM6:hIP^{K297R}	pHM6:hIP^{WT}	5'- CATCCTTTTCCGC***AGG***GCTGTCTTCCAGC -3'
pHM6:hIP^{R302K}	pHM6:hIP^{WT}	5'-GCAAGGCTGTCTTCCAG***AAA***CTCAAGCTCTGGGTCTG -3'
pHM6:hIP^{K304R}	pHM6:hIP^{WT}	5'- CTTCCAGCGACTC***AGG***CTCTGGGTCTGCT -3'
pHM6:hIP^{K297,304R}	pHM6:hIP^{K297R}	5'- CTTCCAGCGACTC***AGG***CTCTGGGTCTGCT -3'

*Oligonucleotide sequences presented correspond to those of the sense primer only; the antisense sequence is inferred. The identity of the mutator codon is in boldface italics with the actual mutated base(s) underlined.

Table 2. Radioligand binding properties of hIP^{WT} or the '*Lys to Gln'* variants expressed in HEK 293 cells.

Receptor	High Affinity Site	Low Affinity Site
	K_d [a]	K_d [a]
hIP^{WT}	3.60 ± 0.23	25.3 ± 4.45
hIP^{K218Q}	2.03 ± 0.40	15.4 ± 1.65
hIP^{K297Q}	2.45 ± 0.35	9.11 ± 1.19
hIP^{K304Q}	3.90 ± 0.23	8.32 ± 0.57
hIP^{K342Q}	3.58 ± 0.67	36.6 ± 0.89
hIP^{K376Q}	2.21 ± 0.63	39.7 ± 5.37
hIP^{K218,297,304,342,376Q}	2.31 ± 0.91	12.7 ± 4.44

[a] nM iloprost.

Scatchard analysis was performed on membrane fractions of HEK 293 cells stably transfected with the human prostacyclin receptor (hIP) or '*Lys to Gln'* variants. Data are presented as the means ± S.E.M. ($n \geq 3$). The suitability of the two affinity state binding model was determined using the F-test to a significance of 0.05.

Table 3. Determination of EC_{50} values for Cicaprost-induced $[Ca^{2+}]_i$ mobilisation.

Receptor	EC_{50} value for Cicaprost-induced $[Ca^{2+}]_i$ * (nM ± S.E.M.)
hIP^{WT}	8.35 ± 1.14
hIP^{K218Q}	18.9 ± 4.41
hIP^{K297Q}	30.3 ± 5.21
hIP^{K304Q}	7.59 ± 1.70
hIP^{K342Q}	21.5 ± 5.97
hIP^{K376Q}	21.3 ± 3.82
$hIP^{K297,304Q}$	30.8 ± 5.50
$hIP^{K297,304,342Q}$	7.97 ± 1.85
$hIP^{K297,304,376Q}$	13.6 ± 2.87
$hIP^{K297,304,342,376Q}$	12.2 ± 2.82
$hIP^{K218,297,304,342,376Q}$	11.0 ± 2.90

*EC_{50} values for cicaprost-induced $[Ca^{2+}]_i$ mobilisation by hIP^{WT} or the '*Lys to Gln'* variants were determined in cells pre-loaded with Fluo-4. Data are presented as the mean changes in $[Ca^{2+}]_i$ ± S.E. ($n \geq 3$).

Figure

Figure 1

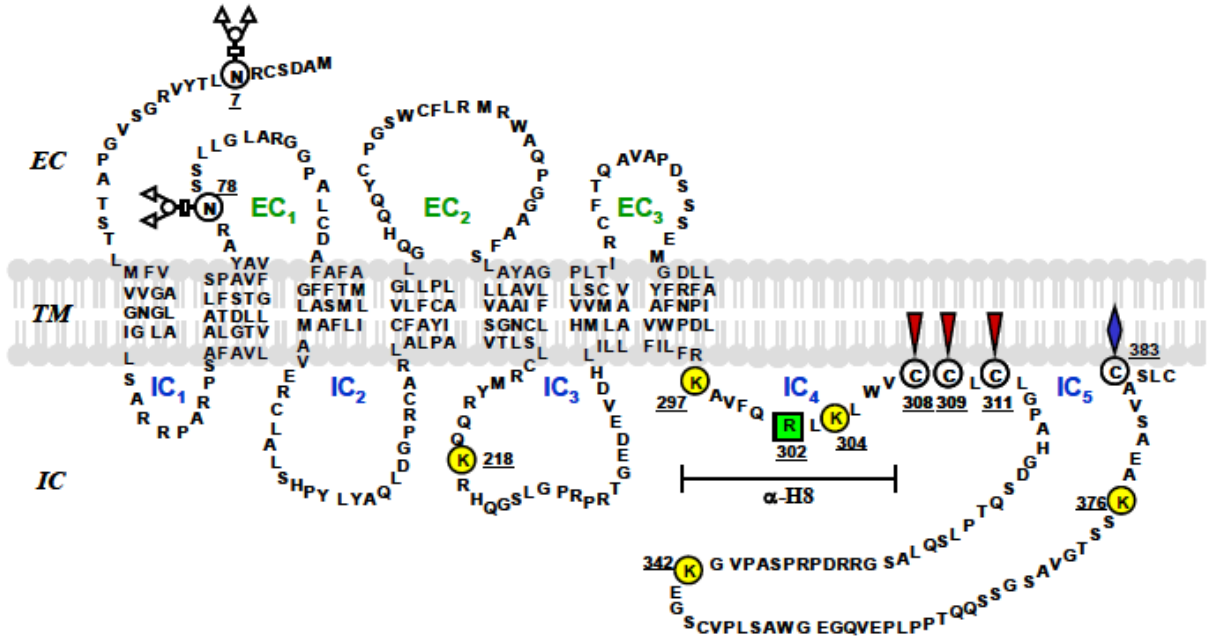

Figure 1. Schematic of the structural organisation of the hIP.
The hIP is predicted to contain an amino (N)-terminal extracellular (EC) domain, seven hydrophobic transmembrane (TM) α-helical domains (TM_1-TM_7) connected by 3 alternating intracellular (IC) loops (IC_1 – IC_3) and 3 EC loops (EC_1 – EC_3) and an IC carboxyl-terminal (C-tail) domain. It is also subject to a number of post-translational modifications including N-linked glycosylation at Asn^{7} and Asn^{78} (represented by the sugar chains); palmitoylation at Cys^{308}, Cys^{309} and Cys^{311} (red triangles), and isoprenylation/farnesylation at Cys^{383} (blue diamond) which together may introduce a double loop structure by creating a fourth (IC_4) and fifth (IC_5) IC loop within the proximal and distal regions, respectively, of the C-tail domain of the hIP. The eighth α-helical domain (α-H8) comprising Lys^{297} – Val^{307} adjacent to the palmitoylated residues at Cys^{308} – Cys^{311}, lying perpendicular to the TM α-helices, is underlined. The hIP contains five Lys residues, Lys^{218} in IC_3 and Lys^{297}, Lys^{304}, Lys^{342} and Lys^{376} in its C-tail domain (yellow circles) while Arg^{302}, between Lys^{297} and Lys^{304} in its proximal C-tail domain, is also highlighted (green square).

Figure 2

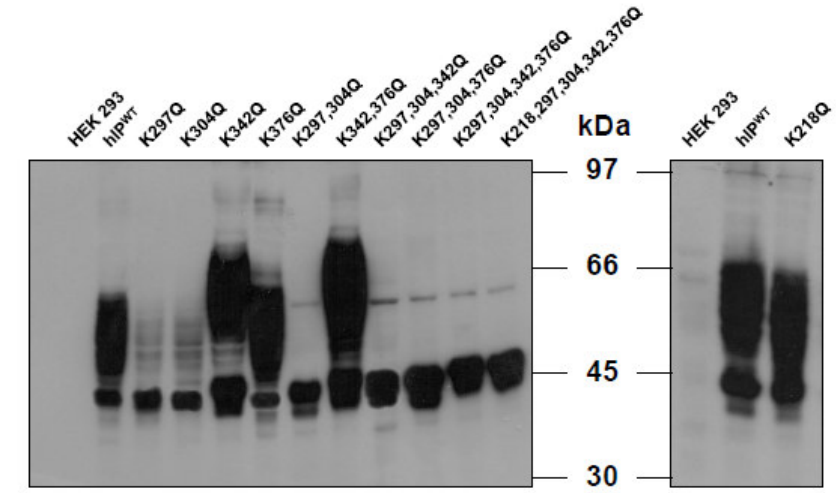

Figure 2

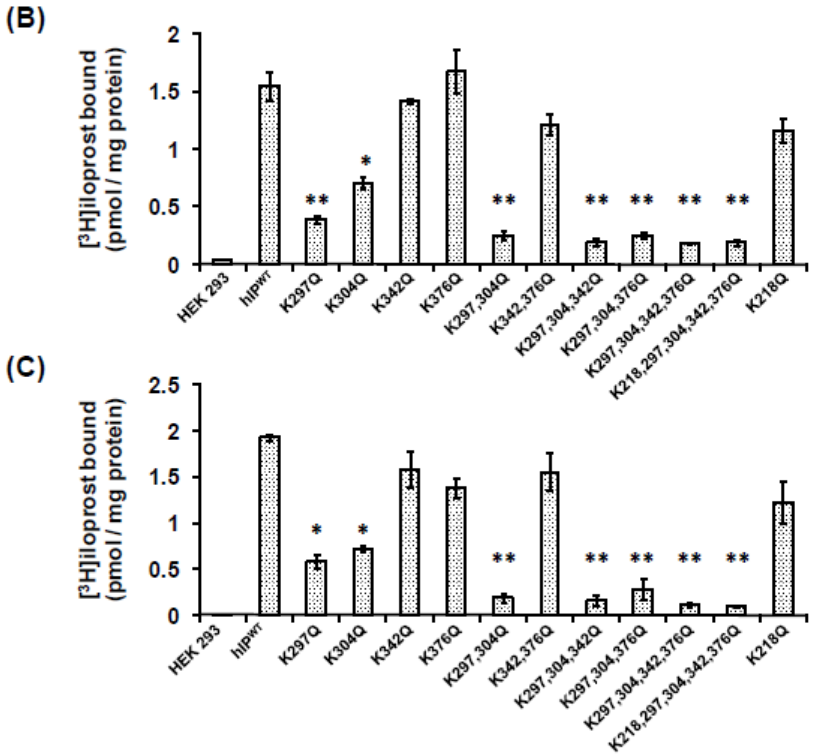

Figure 2

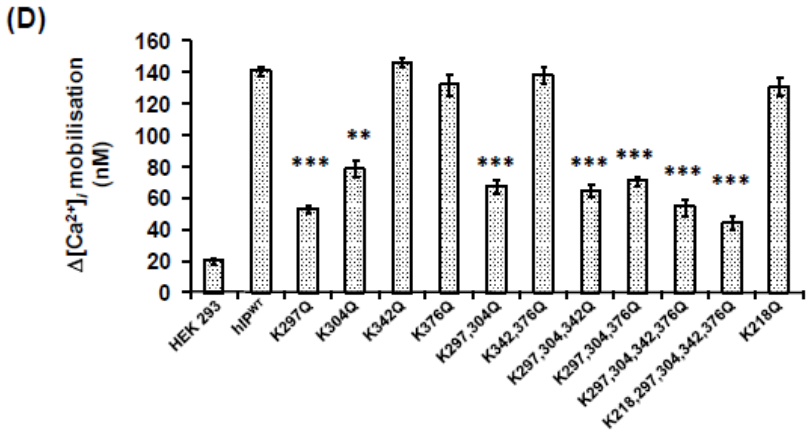

Figure 2

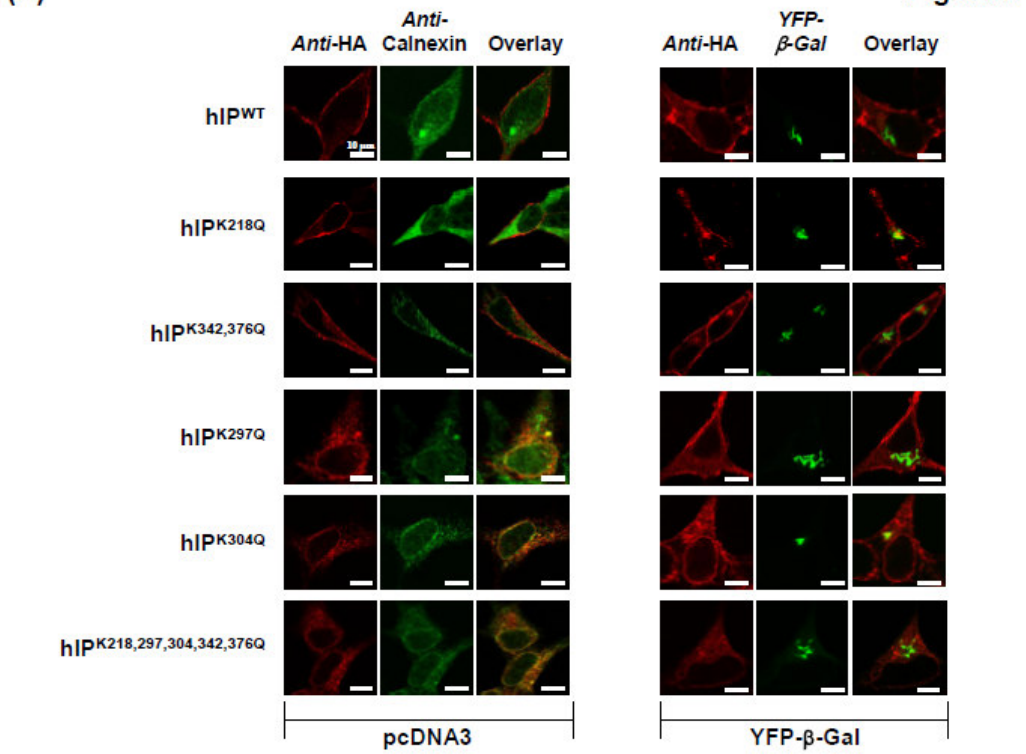

Figure 2. Effect of mutation of the '*Lys to Gln*' residues on the expression & localisation of the hIP.
A. Aliquots (50 µg) of whole cell protein from HEK 293 cells or clonal HEK 293 cell lines stably expressing HA-tagged hIP^{WT} or variant receptors, as indicated, were resolved by SDS-PAGE and immunoblotted versus *anti*-HA (3F10) antibody followed by chemiluminescence detection. The relative positions of the molecular size markers (kDa) are indicated between the panels. Data are representative of three independent experiments. **B & C**. Radioligand binding assays were performed on crude membrane (P_{100}) fractions (**B**) or whole cells (**C**) from the cell types indicated, in the presence of 4 nM [^{3}H]iloprost at 30 °C or 4 °C for 1 hr, respectively, where data is presented as mean [^{3}H]iloprost bound (pmol/mg protein ± S.E.M., n = 4). **D**. Agonist-induced intracellular Ca^{2+} mobilisation in response to stimulation of the cell types indicated with 1 µM cicaprost, where data is presented as mean maximal changes in intracellular Ca^{2+} mobilised ($\Delta[Ca^{2+}]_i$ ± S.E.M., n = 4). **B** - **D**. *, $p < 0.05$; **, $p < 0.01$; & ***, $p < 0.001$ indicates that the mean level of [^{3}H]iloprost bound (pmol/mg protein) or the mean $\Delta[Ca^{2+}]_i$ ± S.E.M. by the various mutant cell lines was significantly reduced in comparison to the wild-type hIP, where applicable. **E.** $HEK.hIP^{WT}$, $HEK.hIP^{K218Q}$, $HEK.hIP^{K342,376Q}$, $HEK.hIP^{K297Q}$, $HEK.hIP^{K304Q}$ and $HEK.hIP^{K218,297,304,342,376Q}$ were transiently transfected with pcDNA3 empty vector (left panels) or with plasmid encoding the Golgi marker YFP-β-Gal (right

panels). Cells were fixed and permeabilised prior to detection of HA-tagged IPs with *anti*-HA 101R/Alexa Fluor® 594 goat *anti*-mouse IgG, calnexin with *anti*-calnexin/Alexa Fluor® 488 goat *anti*-rabbit IgG primary/secondary antibodies, or enhanced yellow fluorescent protein (YFP) expression. In all cases, *anti*-HA, *anti*-calnexin, YFP or overlay images were captured, at x63 magnification, using a Carl Zeiss Lazer Scanning System LSM510 and Zeiss LSM Imaging software. Data presented are representative images from 3 independent experiments from which at least 10 fields were viewed. The white horizontal bar represents 10 μm.

Figure 3

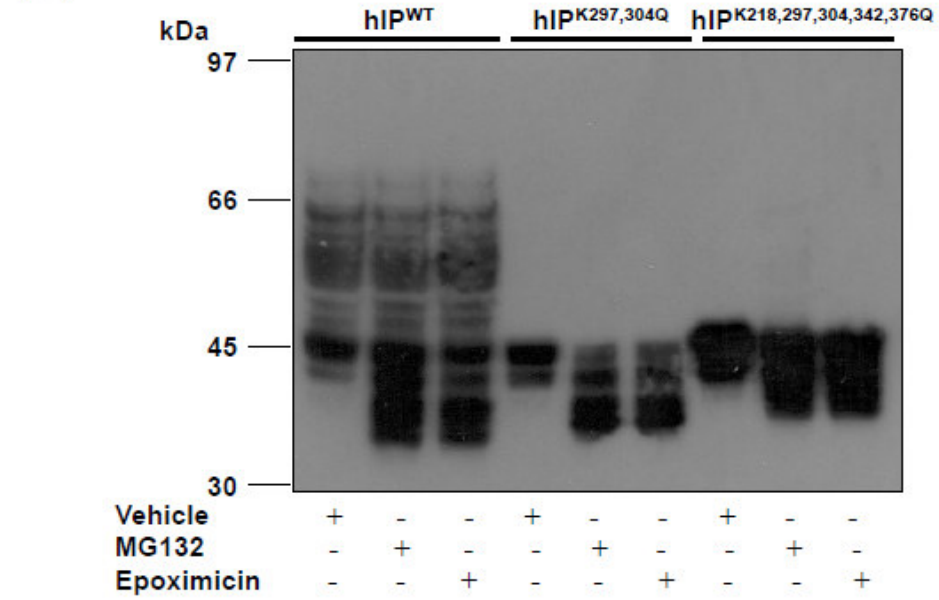

Figure 3

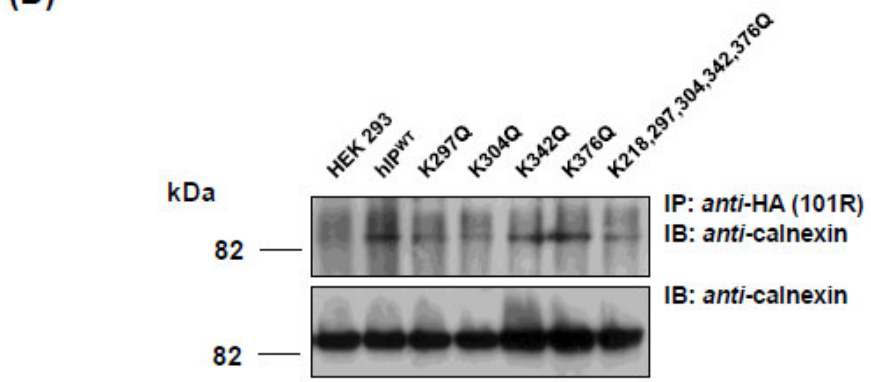

Figure 3. Effect of mutation of the *'Lys to Gln'* on degradation of the hIP through ERAD and interaction with the ER chaperone Calnexin.

A. HEK.hIP^{WT}, HEK.hIP^{K297,304Q} and HEK.hIP^{K218,297,304,342,376Q} cells were treated with 10 μM MG132, 0.1 μM Epoximicin or as control, vehicle for 12 hr. Whole cell proteins (50 μg) were resolved by SDS-PAGE followed by immunoblotting versus *anti*-HA (3F10) antibody. **B.** HA-tagged receptors were immunoprecipitated from HEK 293 cells, clonal HEK 293 cell lines stably expressing HA-tagged hIP^{WT} or mutated hIP variants, as indicated. Immunoprecipitates (IP) were resolved by SDS-PAGE and immunoblotted (IB) versus *anti*-calnexin and *anti*-HA (3F10) antibody followed by chemiluminescence detection. The relative positions of the molecular size markers (kDa) are indicated to the left of the panels. Data are representative of three independent experiments.

Figure 4

(A)

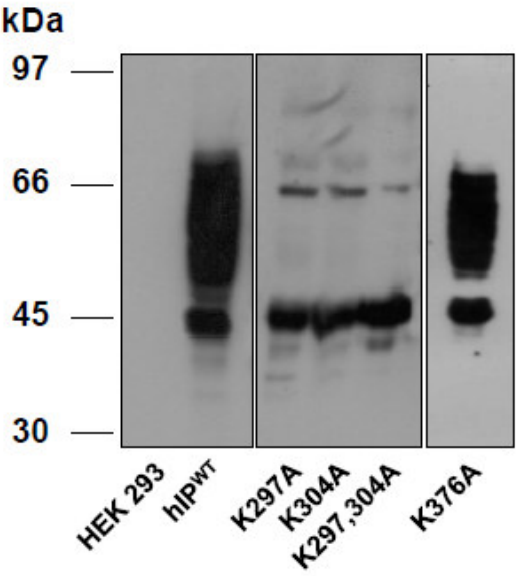

Figure 4

(B)

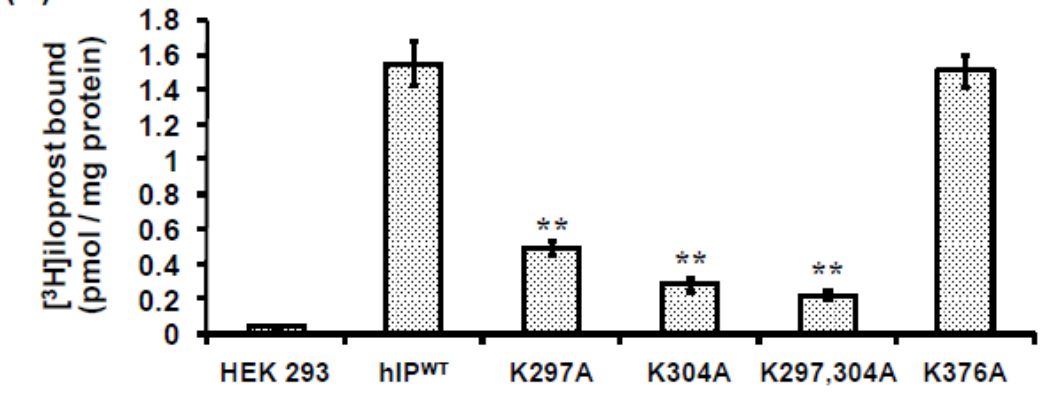

(C)

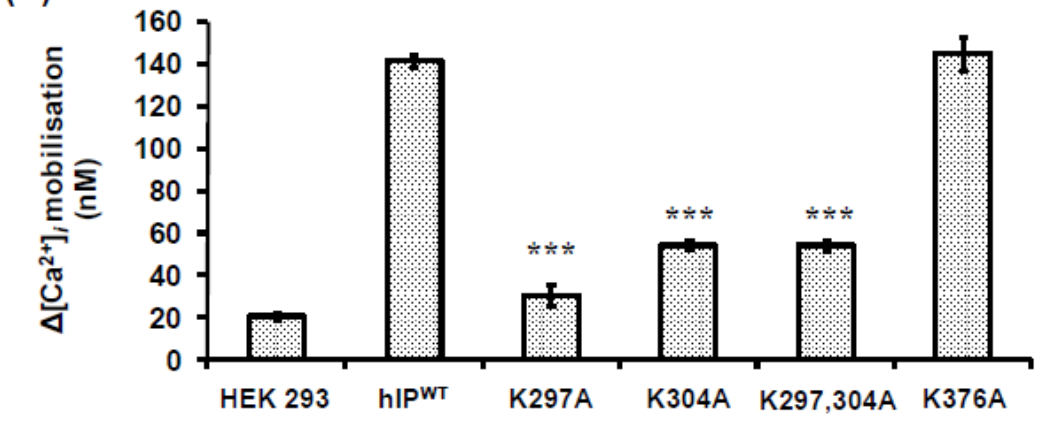

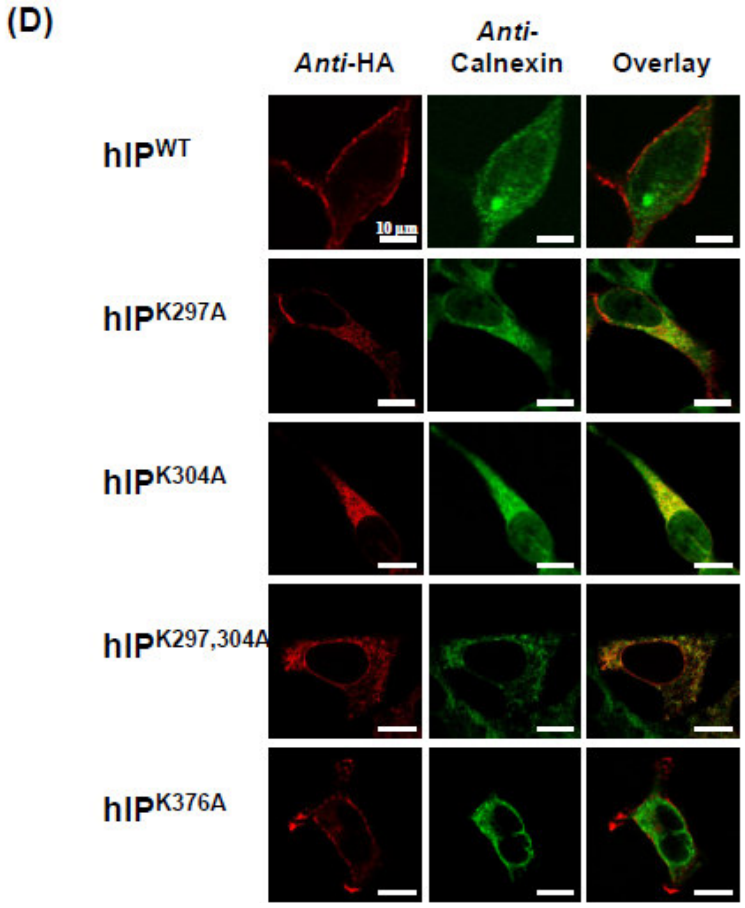

Figure 4. Effect of mutation of the '*Lys to Ala*' residues on the expression & localisation of the hIP.
A. Western blot analysis (50 µg) of whole cell protein from HEK 293 cells or clonal cell lines stably expressing HA-tagged hIP or hIP variants, as indicated. The relative positions of the molecular size markers (kDa) are indicated to the left of the blots. Data presented are representative of three independent experiments. **B**. Radioligand binding assays were performed on crude membrane (P_{100}) fractions from cell types indicated in the presence of 4 nM [^{3}H]iloprost at 30 ^{o}C for 1 hr, where data is presented as mean [^{3}H]iloprost bound (pmol/mg protein ± S.E.M., n = 4). **C**. Agonist-induced intracellular Ca^{2+} mobilisation in response to stimulation of cells with 1 µM cicaprost, where data is presented as mean maximal changes in intracellular Ca^{2+} mobilised ($\Delta[Ca^{2+}]_i$ ± S.E.M., n = 4). **B** & **C**. **, $p < 0.01$ & ***, $p < 0.001$ indicates that the mean level of [^{3}H]iloprost bound (pmol/mg protein) or the mean $\Delta[Ca^{2+}]_i$ ± S.E.M. by the various mutant cell lines was significantly reduced in comparison to the wild-type hIP, where applicable. **D**. HEK.hIP, HEK.hIP^{K376A}, HEK.hIP^{K297A}, HEK.hIP^{K304A} or HEK.hIP^{K297,304A} cells were fixed and permeabilised prior to detection of HA-tagged IPs with *anti*-HA 101R/Alexa Fluor® 594 goat *anti*-mouse IgG or calnexin with *anti*-calnexin/Alexa Fluor® 488 goat *anti*-rabbit IgG primary/secondary antibodies. Images (single or overlay) were captured at x63 magnification using a Carl Zeiss Lazer Scanning System LSM510 and Zeiss LSM Imaging software. Data presented are representative images from 3 independent experiments from which at least 10 fields were viewed. The white horizontal bar represents 10 µm.

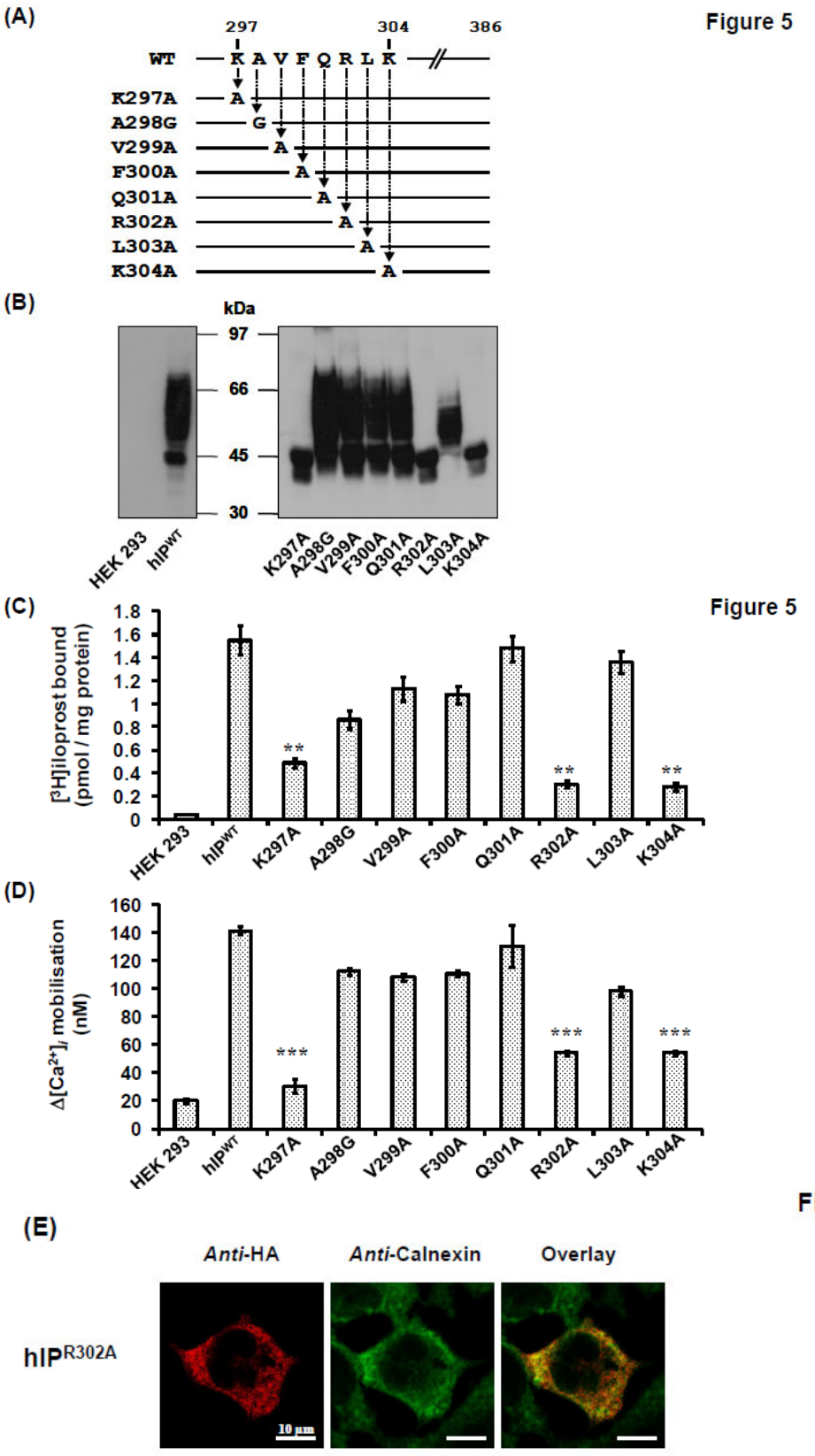

Figure 5. Effect of *Ala-scanning* mutagenesis of Lys^{297} – Lys^{304} on the expression & localisation of the hIP.

A. The sequence of the α-H8 region, from Lys^{297} to Lys^{304}, of wild type hIP is given and the mutations generated are listed. In all cases, *Ala-scanning* mutagenesis was performed with the exception of Ala^{298}

which was mutated to Gly^{298} at that position, to generate hIP^{A298G}. **B.** Western blot analysis (50 μg) of whole cell protein from HEK 293 cells or clonal cell lines stably expressing HA-tagged hIP or hIP variants, as indicated. The relative positions of the molecular size markers (kDa) are indicated between the blots. Data presented are representative of three independent experiments. **C.** Radioligand binding assays were performed on crude membrane (P_{100}) fractions from the cell types indicated in the presence of 4 nM [^{3}H]iloprost at 30 ^oC for 1 hr, where data is presented as mean [^{3}H]iloprost bound (pmol/mg protein ± S.E.M., n = 4). **D.** Agonist-induced intracellular Ca^{2+} mobilisation in response to stimulation of the cell indicated with 1 μM cicaprost, where data is presented as mean maximal changes in intracellular Ca^{2+} mobilised ($\Delta[Ca^{2+}]_i$ ± S.E.M., n = 4). **C & D.** *, $p < 0.05$; **, $p < 0.01$; & ***, $p < 0.001$ indicates that the mean level of [^{3}H]iloprost bound (pmol/mg protein) or the mean $\Delta[Ca^{2+}]_i$ ± S.E.M. by the various mutant cell lines was significantly reduced in comparison to the wild-type hIP, where applicable. **E.** HEK.hIP^{R302A} cells were fixed and permeabilised prior to detection of HA-tagged IPs with *anti*-HA 101R/Alexa Fluor® 594 goat *anti*-mouse IgG or calnexin with *anti*-calnexin/Alexa Fluor® 488 goat *anti*-rabbit IgG primary/secondary antibodies, respectively. Images (single or overlay) were captured at x63 magnification using a Carl Zeiss Lazer Scanning System LSM510 and Zeiss LSM Imaging software. Data presented are representative images from 3 independent experiments from which at least 10 fields were viewed. The white horizontal bar represents 10 μm.

Figure 6

(A)

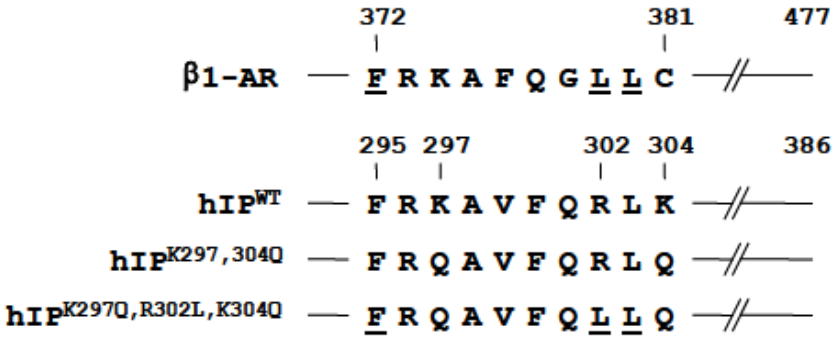

(B) **Figure 6**

(i) **(ii)**

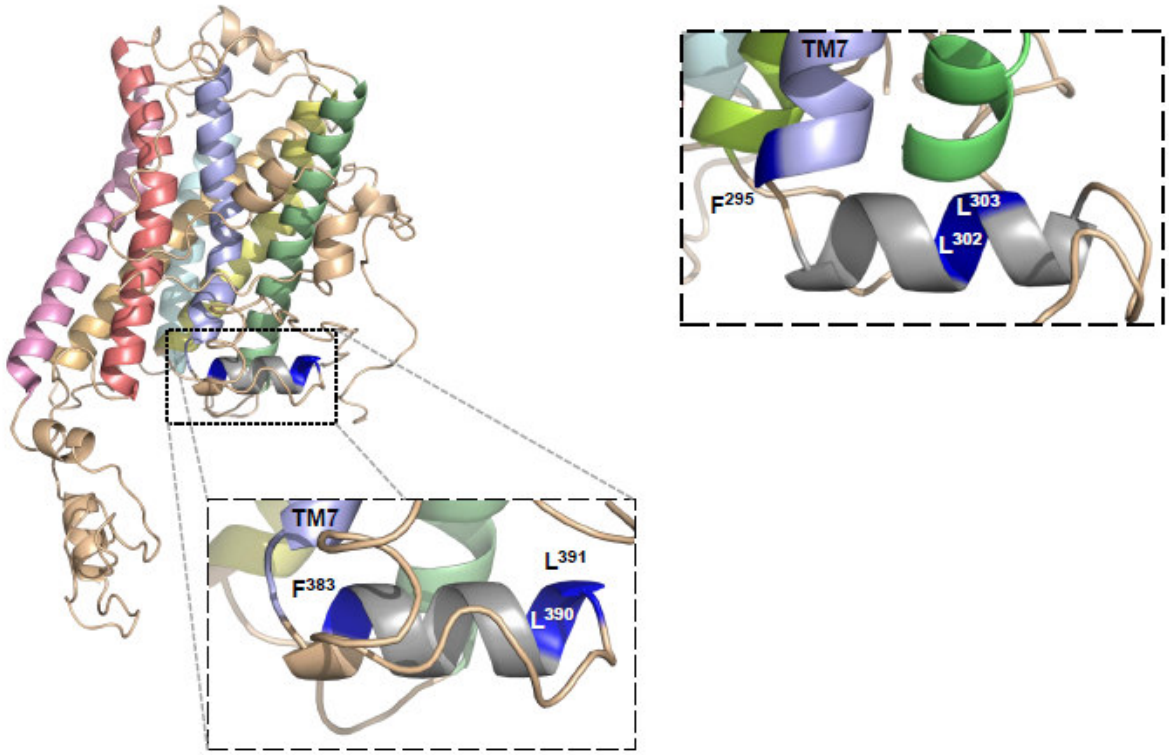

Figure 6

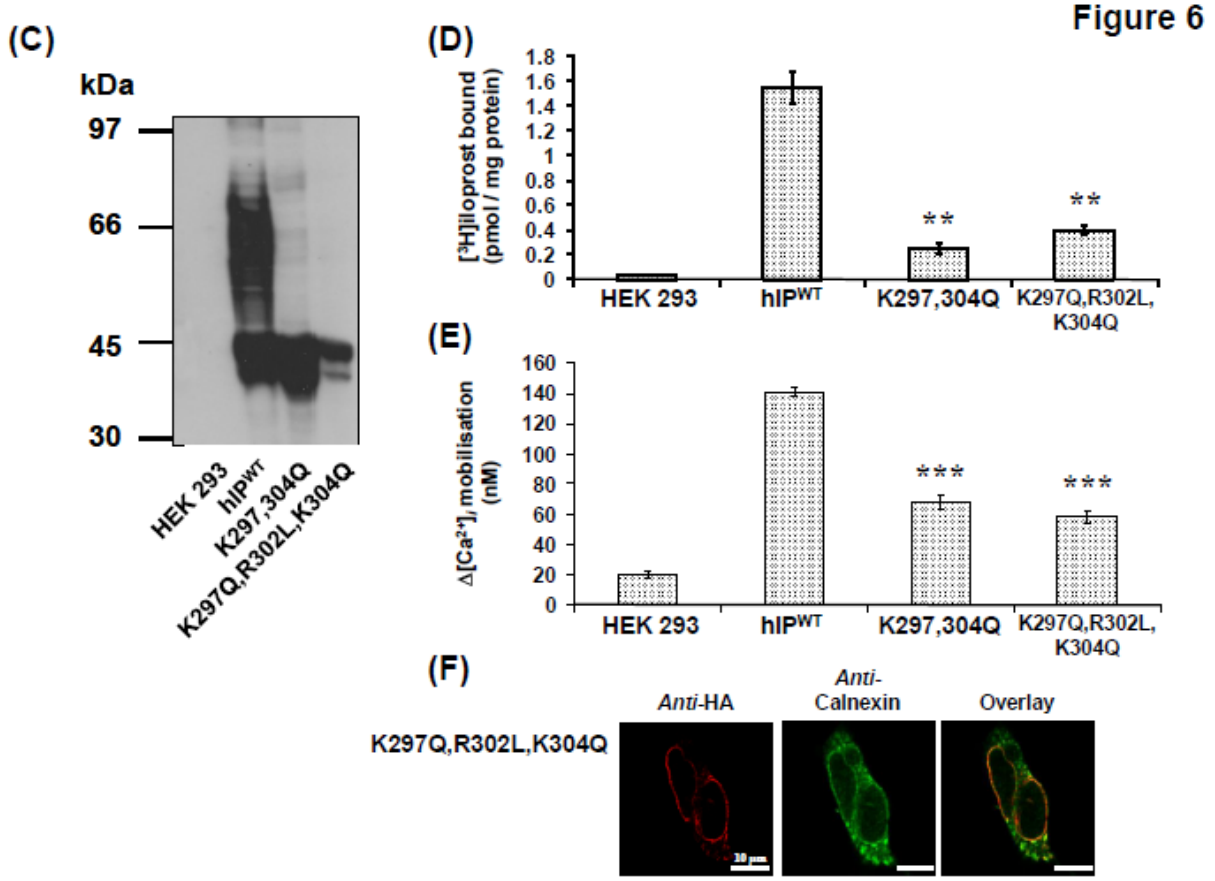

Figure 6. Effect of introducing the 'F(X)$_6$LL' ER export motif on the expression of the hIP^{K297,304Q}. **A.** The amino acid sequence of the proximal C-tail domains of the human β_1-AR (residues 372 – 381), hIP (residues 295 – 304) and its mutated variants, hIP^{K297,304Q} and hIP^{K297Q,R302L,K304Q}, are shown. The core Phe (F) and dileucine (LL) residues located within the canonical F(X)$_6$LL ER motif of the β_1-AR and within the sequence of the hIP^{K297Q,R302L,K304Q} variant are underlined. **B.** I-TASSER three-dimensional structural analyses of the (i) β_1AR and (ii) hIP^{K297Q,R302L,K304Q} predict that they contain 7 TM, typical of their GPCR structure, and that the $F^{383}(X)_6L^{390}L^{391}$ motif of β_1AR (i; inset) and $F^{295}(X)_6L^{302}L^{303}$ of hIP^{K297Q,R302L,K304Q} (ii) lie within the proximal C-tail domains, organised into the eighth α-helical domain (α-H8) of the respective receptors. The overall structure of the β_1AR is presented in (i) while only the region including and surrounding the α-H8 domain of the hIP^{K297Q,R302L,K304Q} is shown in (ii). The defining F and LL residues of the respective F(X)$_6$LL ER motifs are indicated in navy blue in (i) and (ii). **C.** Western blot analysis (50 µg) of whole cell protein from HEK 293 cells or clonal cell lines stably expressing HA-tagged hIP or its mutated variants, as indicated. The relative positions of the molecular size markers (kDa) are indicated to the left of the blots. Data presented are representative of three independent experiments. **D.** Radioligand binding assays were performed on crude membrane (P_{100}) fractions from cell types indicated in the presence of 4 nM [^{3}H]iloprost at 30 ^{o}C for 1 hr, where data is presented as mean [^{3}H]iloprost bound (pmol/mg protein ± S.E.M., n = 4). **E.** Agonist-induced intracellular Ca^{2+} mobilisation in response to stimulation of cell types indicated with 1 µM cicaprost, where data is presented as mean maximal changes in intracellular Ca^{2+} mobilised ($\Delta[Ca^{2+}]_i$ ± S.E.M., n = 4). **D & E.** **, $p < 0.01$ & ***, $p < 0.001$ indicates that the mean level of [^{3}H]iloprost bound (pmol/mg protein) or the mean $\Delta[Ca^{2+}]_i$ ± S.E.M. by the various mutant cell lines was significantly reduced in comparison to the wild-type hIP, where applicable. **F.** HEK.hIP^{K297Q,R302L,K304Q} cells were fixed and permeabilised prior to detection of HA-tagged IPs with *anti*-HA 101R/Alexa Fluor® 594 goat *anti*-mouse IgG or calnexin with *anti*-calnexin/Alexa Fluor® 488 goat *anti*-rabbit IgG primary/secondary antibodies, respectively. Images (single or overlay) were captured at x63 magnification using a Carl Zeiss Lazer Scanning System LSM510 and Zeiss LSM Imaging software. Data presented is a representative image from 3 independent experiments from which at least 10 fields were viewed. The white horizontal bar represents 10 µm.

Figure 7

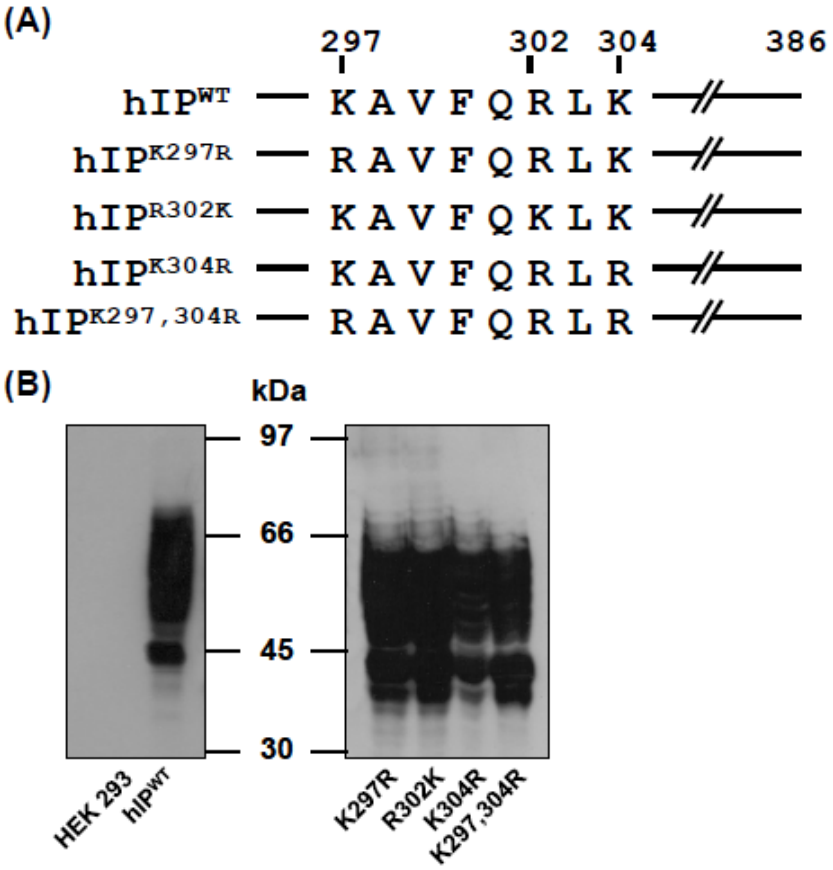

Figure 7

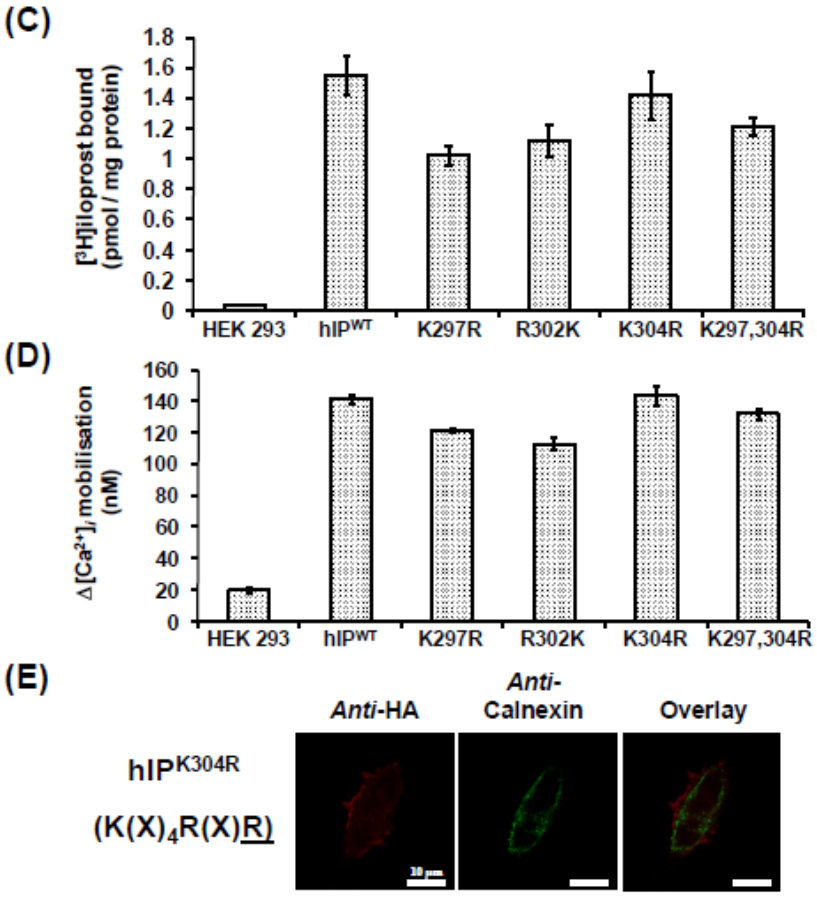

Figure 7. Effect of substituting Lys^{297}, Arg^{302} and Lys^{304} with alternative positively charged residues on expression & signalling of the hIP.

A. The sequence of the wild-type hIP (residues 297 – 304) encoding its putative ER export motif ('$K(X)_4R(X)K$') is given. Below this, the sequence of the various mutations at Lys^{297}, Arg^{302} or Lys^{304} that have been introduced to interrogate whether similarly charged sequences within the variants hIP^{K297R} ('$\underline{R}(X)_4R(X)K$'), hIP^{R302K} ('$K(X)_4\underline{K}(X)K$'), hIP^{K304R} ('$K(X)_4R(X)\underline{R}$') or $hIP^{K297,304R}$ ('$\underline{R}(X)_4R(X)\underline{R}$') might also serve as a functional ER export motif, where the putative motifs are in brackets. **B.** Western blot analysis (50 μg) of whole cell protein from HEK 293 cells or clonal cell lines stably expressing HA-tagged hIP or its mutated variants, as indicated. The relative positions of the molecular size markers (kDa) are indicated between the blots. Data presented are representative of three independent experiments. **C.** Radioligand binding assays were performed on crude membrane (P_{100}) fractions from cell types indicated in the presence of 4 nM [^{3}H]iloprost at 30 ^{o}C for 1 hr, where data is presented as mean [^{3}H]iloprost bound (pmol/mg protein ± S.E.M., n = 4). **D.** Agonist-induced intracellular Ca^{2+} mobilisation in response to stimulation of cell types indicated with 1 μM cicaprost, where data is presented as mean maximal changes in intracellular Ca^{2+} mobilised ($\Delta[Ca^{2+}]_i$ ± S.E.M., n = 4). **E.** HEK.hIP^{K304R} cells were fixed and permeabilised prior to detection of HA-tagged IPs with *anti*-HA 101R/Alexa Fluor® 594 goat *anti*-mouse IgG or calnexin with *anti*-calnexin/Alexa Fluor® 488 goat *anti*-rabbit IgG primary/secondary antibodies, respectively. Images (single or overlay) were captured at x63 magnification using a Carl Zeiss Lazer Scanning System LSM510 and Zeiss LSM Imaging software. Data presented are representative images from 3 independent experiments from which at least 10 fields were viewed. The white horizontal bar represents 10 μm**.**

Figure 8

(A)

	TM 7 / C-tail	
Human	VFILFR**K**AVFQ**R**L**K**LWVCCLCL	312
Mouse	VFILFR**K**AVFQ**R**L**K**FWLCCLCA	339
Rat	VFILFR**K**AVFQ**R**L**K**FWLCCLCA	340
Cow	VFILFR**K**SVFQ**R**L**K**LWFCCLYS	312
Rabbit	VFILFR**K**AVFQ**R**L**K**LWLCCLWP	312
Horse	VFILFR**K**AIFQ**R**L**R**LWFCCLCP	286
Dog	VFILFR**K**AVFQ**K**L**R**LWLCCLGP	311
Chimpanzee	VFILFR**K**AVFK**R**L**K**LWVCCLCL	312
	********::*::*::*:***::	

(B)

	TM 7 / C-tail	
hIP	VFILFR**K**AVFQ**R**L**K**LWVCCLCL	312
hTP	VYILFRRAVLRRLQPRLSTRPR	327
hDP	IFIIFRSPVFRIFFHKIFIRP-	340
hEP_1	VYILLRQAVLRQLLRLLPPRAG	371
hEP_2	VFAILRPPVLRLMRSVLCCRIS	333
hEP_3	VYLLLRKILLRKFCQEMGPDGR	370
hEP_4	IYILLRKTVLSKAIEKIKCLFC	349
hFP	VYILLRKAVLKNLYKLASQCCG	312
	:: ::* ::	

(C)

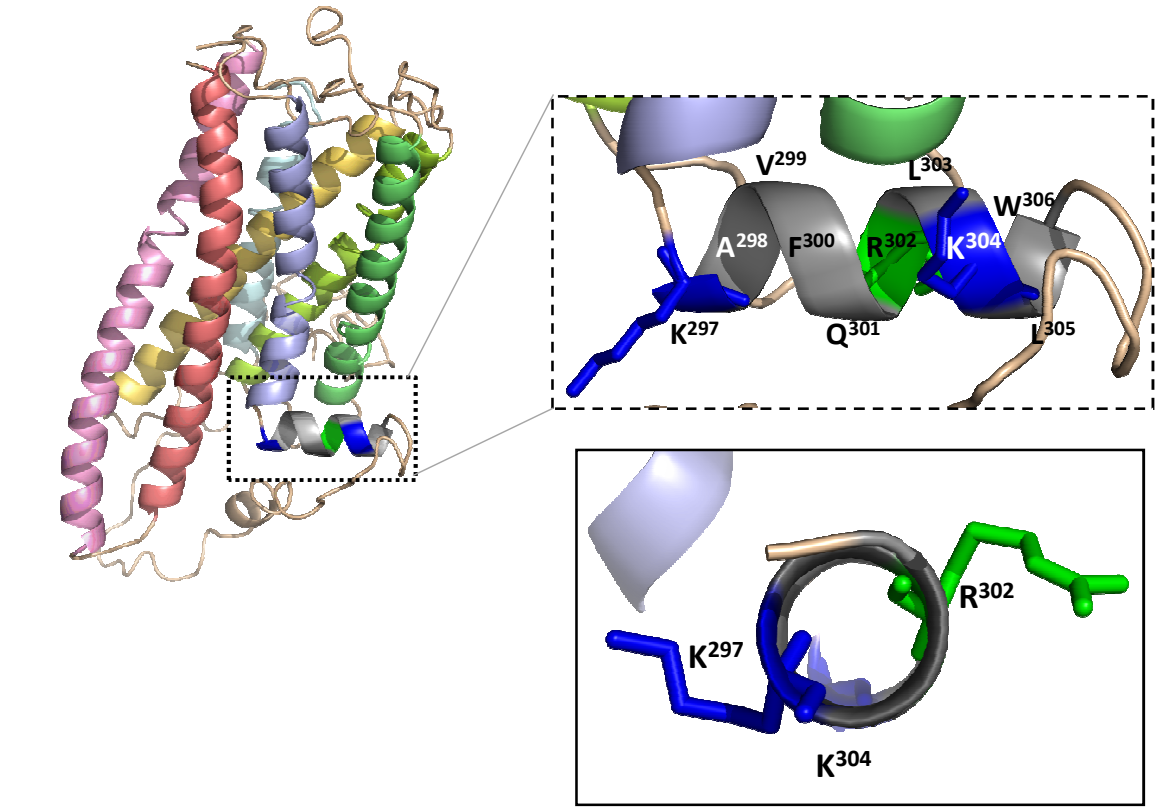

Figure 8. Alignment of Prostacyclin Receptor and human Prostanoid Receptor sequences.
A. The sequence of the human IP (Val^{291} to Leu^{312}) is shown where the critical Lys^{297}, Arg^{302} and Lys^{304} residues of its putative ER export motif ('$K(X)_4R(X)K$') are in bold. Clustal alignment of the equivalent sequence from the IP from seven orthologues reveal that the '$K(X)_4R(X)K$' sequence is conserved in the mouse, rat, cow, rabbit and chimpanzee IP sequences and is replaced by the closely related '$K(X)_4R(X)R$' and '$K(X)_4K(X)R$' sequences within the horse and dog IPs, respectively. **B**. The sequence of the human IP (Val^{291} to Leu^{312}) is shown where the critical Lys^{297}, Arg^{302} and Lys^{304} residues of its putative ER export motif ('$K(X)_4R(X)K$') are in bold. Clustal alignment of the equivalent sequence from the related human (h) prostanoid receptors including the thromboxane receptor (hTP), prostaglandin D receptor (DP), prostaglandin E_1 – E_4 receptors (EP_1 – EP_4, respectively) and the prostaglandin $F_{2\alpha}$ receptor (FP) suggests that the '$K(X)_4R(X)K$' motif is not conserved among the prostanoid receptor family of GPCRs. **A** & **B**. The sequences were aligned to show maximum homology using the Clustal W software [94]. Throughout the alignments, identical amino acids are indicated by asterisks (*****); conservative substitutions are indicated by colons (**:**); and gaps inserted to optimise the alignments are indicated by hyphens (**–**). Sequences are based on the published sequences or on those submitted to the GenBank™/EMBL Data Bank. TM 7, transmembrane domain 7; C-tail, carboxyl-terminal tail domain. **C**. I-TASSER three-dimensional structural analysis of the hIP predicts that it contains 7 TM, typical of its GPCR structure, and that K^{297} – V^{307} (insets; plane and cross-sectional views), within its proximal C-tail domain, is organised into the eighth α-helical domain (α-H8). Data herein establish that K^{297}, R^{302} and K^{304}, within α-H8, form the essential residues of a novel 8 amino acid ER export motif, defined by $K/R(X)_4K/R(X)K/R$, within the hIP, where X represents any amino acid.

Supplemental Figure 1

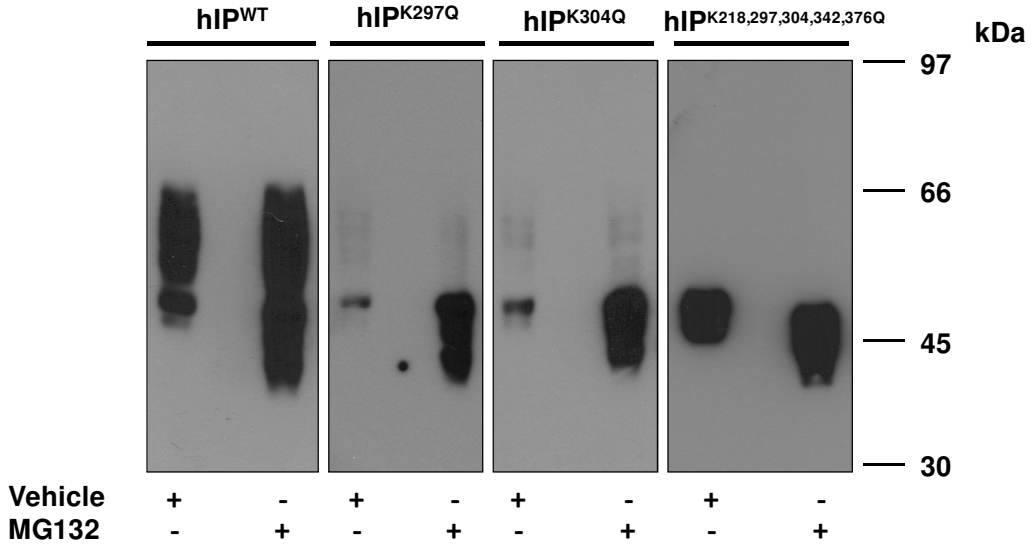

Supplemental Figure 1. Effect of mutation of the Lys to Gln on degradation of the hIP through ERAD.
HEK.hIP^{WT}, HEK.hIP^{K297Q}, HEK.hIP^{K304Q} and HEK.hIP^{K218,297,304,342,376Q} cells were treated with 10 μM MG132 or as control, vehicle for 12 hr. Whole cell proteins (50 μg) were resolved by SDS-PAGE followed by immunoblotting versus *anti*-HA (3F10) antibody. The relative positions of the molecular size markers (kDa) are indicated to the right of the panels. Data are representative of three independent experiments.